atmosphere

MDPI

Article

Atmospheric Ecological Index Prediction and Grade Zoning in the Qinling Mountains Based on Time-Series Models: A Case Study of Shangluo City

Lei Wang [1], Jingyi Chen [1], Xiaogang Li [2,3], Hua Li [4,5,6,*], Shifa Zhao [7], Yaodong Guo [8] and Xiaocun Zhang [2]

[1] School of Modern Agriculture and Bioengineering, Shangluo University, Shangluo 726000, China; wangleiwine@slxy.edu.cn (L.W.); chenjingyi@stu.slxy.edu.cn (J.C.)
[2] School of Urban and Rural Planning and Architectural Engineering, Shangluo University, Shangluo 726000, China
[3] Ecohydrology Observation and Research Station of the Southern Qinling Mountains, Shangluo 726000, China
[4] College of Enology, Northwest A&F University, Xianyang 712100, China
[5] Shaanxi Engineering Research Center for Viti-Viniculture, Xianyang 712100, China
[6] China Wine Industry Technology Research Institute, Yinchuan 750021, China
[7] Shangluo Meteorological Bureau, Shangluo 726000, China
[8] College of Health and Physical Education, Shangluo University, Shangluo 726000, China
* Correspondence: lihuawine@nwsuaf.edu.cn

Abstract

Mountain ecosystems are sensitive response units and critical ecological barriers to global climate change. Located in the mid-latitude climate transition zone, these ecosystems feature high ecological sensitivity and complex driving mechanisms, creating an urgent need to conduct long-sequence, high-precision dynamic assessments in order to support ecological conservation and climate adaptation decision-making. However, three key research gaps remain in the field: first, traditional assessments are dominated by static observation, lacking the capacity for long-sequence dynamic analysis and future projection; second, the coupled interaction mechanism among multiple ecological factors remains unclear, with insufficient quantitative and physical mechanism characterization; third, existing ecological zoning has not been validated for robustness, rendering it incapable of addressing climate disturbances and extreme scenarios. In order to study the regional atmospheric ecosystem, this study takes Shangluo in the eastern Qinling Mountains as the study area and constructs an integrated assessment framework integrating multi-dimensional diagnosis, simulation and projection, dynamic zoning and robustness validation based on long-sequence multi-factor data covering the years 1965–2024. The study aims to reveal the long-sequence evolution patterns and four-dimensional coupling mechanism of the Qinling Mountains atmospheric ecosystem, developing a reproducible and transferable dynamic assessment model. The results show that the study area exhibits the characteristic of elevation-dependent warming, and the correlation coefficients between elevation and air temperature, and between vegetation coverage and air quality reach −0.89 and −0.76, respectively.; ecological quality presents a spatial pattern of being high in the southwest and low in the northeast, with a coefficient of variation across the whole study area lower than 0.03. The results of 1000 Monte Carlo random disturbance validation runs show that even under intensified climate stress, the zoning pattern still maintains extremely strong disturbance resistance. This study reveals the steady-state multi-factor interaction mechanism in mountainous regions, addressing the defects of traditional static assessments that ignore ecosystem evolution and lag effects. The dynamic projection model constructed in this study can be transferred to similar mid-latitude mountainous regions worldwide, providing theoretical and technical support for regional ecological governance.

Academic Editors: Jianghua Wu and Gareth Marshall

Received: 27 January 2026
Revised: 4 June 2026
Accepted: 5 June 2026
Published: 9 June 2026

Keywords: mid-latitude transition zone mountains; altitude-dependent warming; long-term dynamic assessment; four-dimensional coupling mechanism; spatiotemporal zoning

1. Introduction

Mountain ecosystems are the most sensitive indicators of global climate change, playing a crucial role in ecological buffering and protection [1]. Under the multiple disturbances of global warming, frequent extreme weather events, and intensified human activities in mountainous areas, the global mountain atmospheric ecological pattern is constantly reshaping [2], which is a critical issue in current climate and ecological research. The mountainous areas in the mid-latitude climate transition zone have a fragile ecological background and a highly sensitive atmospheric environment. Their atmospheric ecological evolution is jointly regulated by topography, climate, vegetation, and human activities [3], and there is an urgent need for long-term, high-precision dynamic assessment to provide scientific support for refined mountain ecosystem management. At present, across the globe, mainstream mountain atmospheric ecological assessment methods generally follow a traditional research paradigm, driven by experience and static discrete analysis [4–6] and mostly constructed for ordinary mountains with homogeneous and simple topography, with a fixed system and strong universality. However, climate transition zone mountains feature unique characteristics such as element abruptness, spatial heterogeneity, and nonlinear system superposition [7]. The traditional paradigm has inherent structural deficiencies in mechanism description, spatiotemporal prediction, and multi-factor coupling adaptation, meaning it cannot adapt to the complex ecological evolution laws of the transition zone mountains. This also makes it necessary to adapt the assessment paradigm specifically for the transition zone.

As a national core ecological barrier marking the climate divide between the north and south of China, the Qinling Mountains have a typical complex transition zone ecosystem and are highly sensitive to external disturbances in the atmospheric ecosystem [8]. In recent years, the rapid expansion of the regional tourism and health care industries has led to changes in land use patterns and increased human activity disturbances, continuously threatening local atmospheric ecosystem stability [3,9]. At the same time, the standards for regional ecological management have been continuously upgraded, which has created higher requirements for the temporal evolution analysis, quantitative assessment, and future scenario prediction of atmospheric ecological quality. High-precision dynamic assessment has become the core decision-making basis for ecological management and industrial layout optimization in the Qinling Mountains [10]. Compared with conventional mountains, the driving factors of the atmospheric ecosystem in the Qinling transition zone are interlocked, and the evolution process is highly non-stationary. The fixed assessment logic of the traditional paradigm further amplifies the methodological adaptation error. Existing studies are difficult to adapt to the complex system characteristics of the transition zone mountains; they have significant methodological and cognitive deficiencies, which means they cannot support high-quality regional ecosystem governance.

The traditional mountain atmospheric ecological assessment paradigm currently used in sensitive mountain areas is characterized by static snapshot evaluation, independent single-factor analysis, purely data-driven modeling, and fragmented regional analysis. However, there are four core scientific deficiencies in this research field: First, the static assessment paradigm lacks the ability to provide a dynamic analysis over time. Existing studies mostly conduct static evaluations based on instantaneous cross-sectional data, which can only reflect the current ecological snapshot [11] and cannot effectively describe

the interannual fluctuation patterns and long-term evolution trends in atmospheric ecological quality [12,13]. It lacks medium- and long-term prediction capabilities and ignores the dynamic evolutionary nature of the mountain atmospheric ecosystem, resulting in insufficient systematicness and assessment result timeliness. Second, the multi-factor coupling and mutual feedback mechanism has not been systematically revealed and quantitatively characterized. Existing studies have not systematically elucidated the multi-dimensional nonlinear coupling and two-way mutual feedback mechanism among terrain, climate, vegetation and air quality, making it difficult to quantitatively distinguish each factor's independent contribution and synergistic regulation effect [14,15]. Moreover, time-series models that integrate both physical constraints and robust predictive capability remain scarce [16]. Third, the robustness and reproducibility of current time-series modeling are relatively weak. Traditional time-series analysis lacks a complete robustness testing system, which makes it difficult to guarantee analytical result credibility [17]. Although data-driven models demonstrate satisfactory fitting performance, they suffer from insufficient physical mechanism embedding and prominent black-box problems, leading to poor model generalization and cross-regional transferability, and no standardized modeling and validation paradigm has been established. Fourth, the current research system is fragmented and lacks integration. Although existing studies have broken down the inherent correlation among time-series diagnosis, predictive modeling and ecological regionalization, no unified assessment framework has been formed [18]. Most ecological regionalization schemes are statically delimited based on current status; a methodological system for dynamic ecological regionalization adaptive to future climate disturbances has not been established, and multi-scenario robustness verification is lacking, all of which limit the practical application value of regionalization results [4,19].

The aforementioned shortcomings represent inherent structural limitations of the traditional paradigm. Simply optimizing algorithms and expanding data cannot fundamentally resolve the issues of assessment distortion, unclear mechanisms, and poor applicability in mountainous areas located within climatic transition zones, which constrain the standardized, precise development of atmospheric ecological assessments for sensitive mountainous regions. How can the long-term sequential evolution laws of atmospheric ecosystems in transition zone mountains be accurately characterized? How can reliable predictions of future scenarios be achieved? How do the four dimensions of "terrain–climate–vegetation–air quality" implement nonlinear coupling and two-way interaction, jointly driving atmospheric ecological pattern formation? How can a time-series prediction model that combines both physical mechanism constraints and high robustness be constructed to improve the model's generalization ability and regional transferability? How can a dynamic ecological zoning system oriented to future climate disturbances be established? How can the long-term applicability of zoning results be guaranteed using robustness testing? These core scientific questions remain urgent, unanswered issues in the field of atmospheric ecology.

This study takes the mountainous area of the eastern Qinling climate transition zone as the object, constructing an integrated framework of "multi-dimensional time-series diagnosis-mechanism-constrained prediction-dynamic zoning under climate disturbance". Four targeted research goals are set: (1) to identify the long-term spatiotemporal evolution characteristics and differentiation laws of key atmospheric ecology indicators in the eastern section of the Qinling Mountains in Shangluo City from 1965 to 2024, addressing the deficiencies of traditional static assessment that emphasize current status over dynamic evolution; (2) to quantitatively analyze the coupling and feedback mechanisms of the four-dimensional system of terrain, climate, vegetation, and air quality, clarifying the independent contributions and coordinated regulatory roles of each main control factor;

(3) to construct an atmospheric ecological index (AEI) constrained by physical mechanisms and an optimized AutoRegressive Integrated Moving Average (ARIMA) prediction model, conducting comparative analysis with traditional static assessment methods and unconstrained time-series models to verify the prediction accuracy and robustness of the new model; and finally (4) to predict the evolution trend of the regional atmospheric ecological pattern from 2025 to 2040, carrying out dynamic grade zoning and verifying its robustness through multi-scenario Monte Carlo simulation, thus forming a high-credibility zoning plan that can support ecological management.

Compared with traditional methods, the new atmospheric ecological assessment paradigm proposed in this study achieves four-dimensional innovations: (1) shifting from instantaneous static cross-sectional evaluation to long-term dynamic evolution analysis; (2) moving from the independent assessment of single elements to four-dimensional coupling and feedback analysis of terrain, climate, vegetation, and air quality; (3) transitioning from purely data-driven to physical mechanism constraints combined with optimized ARIMA time-series prediction; and (4) evolving from fragmented analysis to an integrated closed loop of multi-dimensional diagnosis, simulation prediction, dynamic zoning, and robustness verification.

The atmospheric ecosystem in Shangluo City, eastern Qinling Mountains, is characterized by overall high stability and robustness. Regulated by elevation-dependent warming and the four-dimensional coupled negative feedback mechanism of terrain–climate–vegetation–air quality, the regional AEI shows a stable spatial pattern of excellence in the southwest and weakness in the northeast; it remains unchanged in grade even under future climate disturbance scenarios, demonstrating strong anti-interference ability. This study confirms that although high-altitude mountainous areas show more significant warming, they form a remarkable thermal buffering effect under the combined action of closed terrain and high vegetation coverage, and their ecological stability is superior to that of low-altitude areas. It revises the traditional cognition that "higher elevation means more fragile ecology" from a mechanistic perspective. The long-term dynamic assessment and robust zoning model constructed in this study have satisfactory prediction accuracy and regional transferability, which can provide scientific support and paradigm reference for atmospheric ecological protection, dynamic zoning and climate adaptation governance in mid-latitude climate transition mountainous areas worldwide.

2. Methods

2.1. Study Area and Data Processing

In this study, Shangluo City, located in the eastern section of the Qinling Mountains, was selected as the research area. This region is a typical ecologically sensitive mountainous area in China, constituting a key ecological barrier of the Qinling Mountains. Shangluo City lies between 33°02′ N and 34°24′ N and 108°34′ E and 111°01′ E, with jurisdiction over six counties (Zhashui, Shangnan, Zhen'an, Danfeng, Shanyang and Luonan), as well as Shangzhou District. The geographical location of the study area is shown in Figure 1. For this study, long-term data from seven core atmospheric ecological indicators were collected from the Shangluo Meteorological Bureau and the Geospatial Data Cloud platform of the Chinese Academy of Sciences. Data preprocessing procedures included missing value interpolation, outlier correction and standardization processing. The dataset was divided into training and test subsets, which were used for model construction and independent validation, respectively.

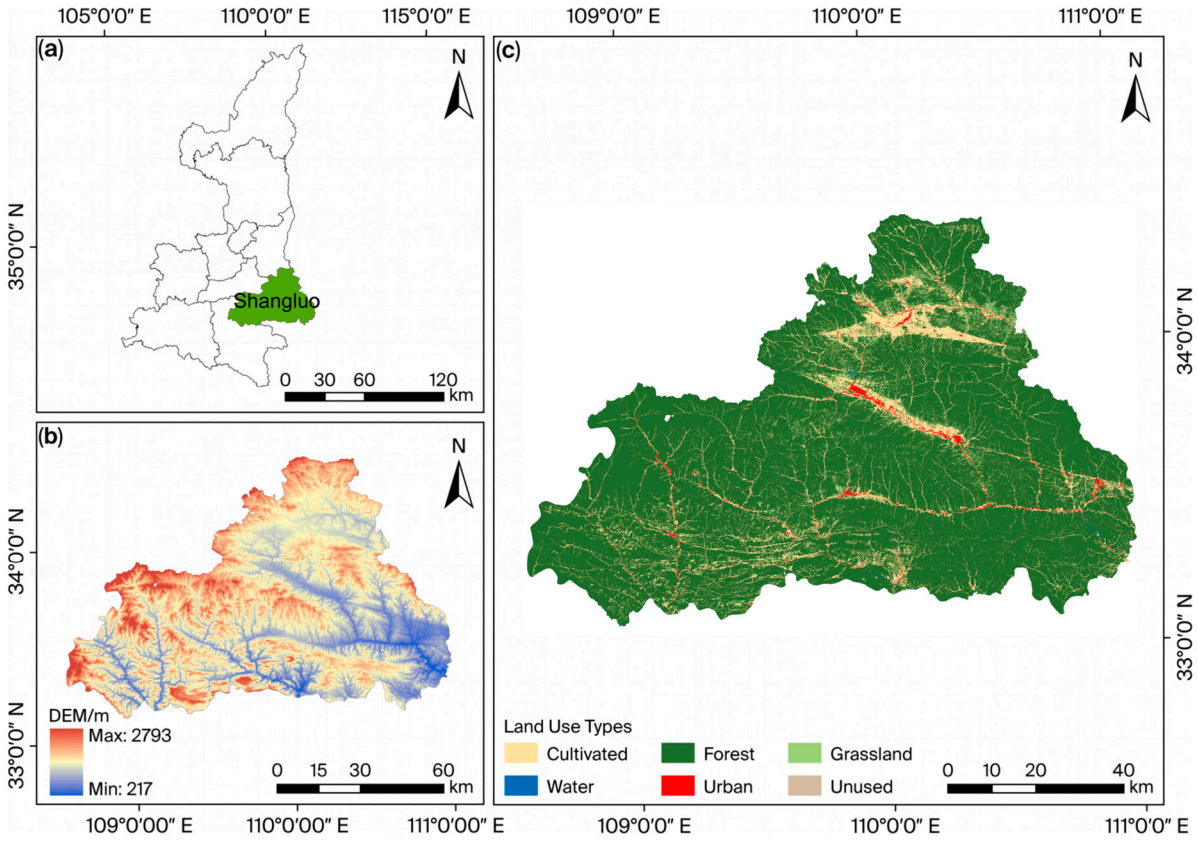

Figure 1. Spatial distribution of basic geographical elements in the study area of Shangluo City, Shaanxi Province. (**a**) Schematic diagram of the geographical location of Shangluo City, Shaanxi Province; (**b**) Spatial distribution of elevation (DEM) in Shangluo City, Shaanxi Province; (**c**) Spatial distribution of land use types in Shangluo City, Shaanxi Province.

The study utilized a long-term multi-element dataset from 1965 to 2024, incorporating seven core indicators. Among them, the observation sequences of temperature, precipitation, relative humidity, and sunshine duration fully covered the period from 1965 to 2024, with data sourced from the Shangluo Meteorological Bureau (one of the authors of this study is affiliated with this institution, and data acquisition was conducted in compliance with regulations). These data underwent homogenization correction and multi-level quality control, and the observation standards and data accuracy conformed to national meteorological observation standards. The Normalized Difference Vegetation Index (NDVI) remote sensing data (https://www.resdc.cn), which underpinned the vegetation coverage index, had continuous and stable observations since 1981, with no valid satellite-based vegetation observation records before 1981. The Air Quality Index (AQI) was officially monitored in a standardized manner starting from 2013, and there were no unified standard observation sequences before this time. The elevation data were derived from a Digital Elevation Model (DEM) product with uniform resolution, sourced from the Geospatial Data Cloud Platform of the Chinese Academy of Sciences (https://www.gscloud.cn/search, accessed on 6 November 2025), and used to represent topographic constraints. Data processing and Monte Carlo simulations were implemented using Python version 3.12 (https://www.python.org); spatial maps of the study area were created and visualized with ArcGIS version 10.8 (https://www.arcgis.com).

To ensure the data's spatial representativeness, research samples covered high-altitude mountains; mid–low mountains and hills, river valleys and basins; and urban built-up areas throughout the city, fully taking into account the differences in topographic, vegetation, and human activity intensity gradients, ensuring that the results could reflect the region's

overall atmospheric ecological characteristics. A standardized preprocessing procedure was applied to all data: abnormal values were identified and removed using the 3σ principle; short-term missing values were filled using a combination of weighted interpolation from neighboring stations and linear interpolation [20,21]; all indicators were standardized to the 0–1 interval to eliminate the influence of dimensional differences on the assessment results [22]; and finally, for the needs of time-series modeling, non-stationary sequences were preprocessed to achieve stationarity, ensuring reliability in the subsequent statistical analysis and model fitting [23].

2.2. Construction of Indicator System and Determination of Weights

In this study, seven indicators—air temperature, precipitation, relative humidity, sunshine duration, fractional vegetation cover, AQI and altitude—were selected to establish an atmospheric ecological assessment indicator system. Each indicator possesses clear physical and climatic implications, and can systematically characterize the thermal condition, hydrological regime, radiation regime, vegetation support, air quality and topographic constraint attributes of the atmospheric ecosystem [24,25]. These quantifiable metrics are widely adopted in global mountain climate and ecological research, with favorable repeatability and comparability.

The weights of all indicators were determined via the analytic hierarchy process (AHP) combined with the expert scoring method. A total of 50 experts with long-term research experience in mountain meteorology and climatology, ecological environment, and natural resource assessment of the Qinling Mountains were invited to conduct importance scoring for each indicator. The rationality and reliability of weight allocation were verified by a consistency test, with Consistency Ratio (CR) < 0.1, thereby eliminating single subjective weighting-induced bias [26,27]. All standardized indicators were linearly weighted and integrated based on the optimized weight coefficients to construct the atmospheric ecological index, which was applied for comprehensive and quantitative regional atmospheric ecological quality evaluation. The Analytic Hierarchy Process (AHP) is a multi-criteria weight determination method that hierarchizes and structures complex decision-making problems. First, the evaluation system is decomposed into a three-level structure consisting of the target layer, criterion layer, and index layer. Subsequently, experts conduct pairwise comparisons on the relative importance of each indicator to construct a judgment matrix. The maximum eigenvalue and corresponding eigenvector are calculated based on the matrix to obtain the initial weights of each indicator. Finally, the logical consistency of the judgment matrix is tested via the consistency ratio (CR): when CR < 0.1, the obtained weights are considered valid, and ultimately a scientific, stable and repeatable indicator weight result is obtained [26,27].

Expert selection was strictly implemented following four principles: professional matching, working seniority, research qualification and regional adaptability. All participating experts hold a professional title of associate senior or above, or a doctoral degree, with no less than 8 years of research experience in relevant fields. They have long devoted themselves to research in climatic evolution, atmospheric ecology, and coupling mechanisms between vegetation and the environment in the Shangluo area of the Qinling Mountains, meaning they are well acquainted with the region's physical geography and meteorological observation characteristics. The expert panel covers researchers and practitioners from universities, research institutes, meteorological administrations and ecological environment monitoring institutions, featuring a rational professional structure and diverse research perspectives. This ensures the scientificity, objectivity and regional applicability of indicator scoring, meeting the professional evaluation criteria for weight assignment in the AHP framework.

Indicator weights were determined using the analytic hierarchy process combined with expert scoring, and a correlation heatmap of expert scores is shown in Appendix B, Figure A1, with consistency tests to ensure reliability. The atmospheric ecological index was established as a linear weighted composite of standardized indicators, and a grading system was defined based on long-term regional characteristics.

2.3. Time-Series Diagnosis and ARIMA Model Construction

To ensure the standardization of analysis and the reliability and reproducibility of modeling results, this study constructs a complete time series diagnosis procedure. First, the Augmented Dickey–Fuller (ADF) unit root test is employed to identify the stationarity of the original time series. The test specification includes a constant term and excludes the time trend term, and the stationarity of the series is determined based on the p-value of the test, which provides a basis for subsequent differential processing of the data [28]. Second, the Ljung–Box white noise test is applied to analyze the autocorrelation of the series, with a uniform lag order of 20 set to judge whether the series has valid temporal correlation characteristics, thereby eliminating random sequences with no research value. In this study, the Mann–Kendall nonparametric test is adopted to identify the change trend and mutation points of the time series data, and the sliding t-test is combined to accurately determine the location of mutations. Implicit periodic information is extracted based on the fluctuation pattern of the series, which reduces the judgment error caused by a single test and improves the stability of trend identification results [29]. To distinguish the effects of different driving factors on time series data, the original time series is decomposed into trend component, seasonal component and residual component via the Seasonal-Trend decomposition using Loess (STL) seasonal decomposition algorithm, revealing the long-term evolution pattern, seasonal fluctuation characteristics and random disturbance variation in the data, respectively [30]. The significance level for all statistical tests in this study is set at 0.05, and the test result is considered statistically significant when $p < 0.05$.

This study selects the ARIMA model to implement time series prediction. To ensure objective and reasonable model evaluation, the dataset is divided at a ratio of 7:3. The first 70% of the time-ordered data is used as the training set for model fitting, and the remaining 30% is used as an independent test set to verify model accuracy. The original temporal order of the data is not disrupted during the division process. The model parameters (p, d, q) are determined through an objective approach: the difference order d is determined based on the ADF test results to ensure that the processed series meets the stationarity requirement; the grid search method is used to traverse the reasonable parameter interval, and the minimum Akaike information criterion (AIC) is adopted as the screening criterion to determine the optimal autoregressive order p and moving average order q, which reduces the subjective bias caused by manual parameter setting [31]. After model training is completed, a rationality test is conducted on the residuals, including a normality test, Ljung–Box autocorrelation test, to ensure that the residuals satisfy the statistical requirements of independence, no autocorrelation and homoscedasticity, avoid problems of overfitting, underfitting and systematic errors, and guarantee the authenticity and reliability of prediction results [32].

2.4. Spatial Analysis, Ecological Zoning and Coupling Analysis

Spatial pattern analysis was carried out based on the atmospheric ecological index. Combined with differences in altitude, underlying surface type and human activity intensity [19,33], the regulatory effects of terrain and regional differences on the atmospheric ecological pattern were fully considered. According to the numerical distribution of the atmospheric ecological

index, a grading standard was constructed, and atmospheric ecological zoning was carried out to spatially delineate the ecological types in the study area.

Pearson correlation analysis [34] was used to quantitatively analyze the coupling correlation characteristics among the multiple elements of terrain–climate–vegetation–air quality, identify the mutual feedback direction between key driving factors and elements, and provide a quantitative basis for the atmospheric ecological pattern formation mechanism.

2.5. Stability and Robustness Assessment

To verify the reliability and anti-disturbance ability of the ecological zoning results, this study adopted the coefficient of variation method to evaluate the temporal stability of the atmospheric ecological index [13,35]. Meanwhile, a Monte Carlo random disturbance simulation was applied to examine the hierarchical stability of the zoning results under random interference by setting multiple groups of climate disturbance scenarios; in this way, we characterized the zoning scheme's robustness [36,37]. Constrained by the historically observed extreme values in the study area, random parameter disturbances were performed on core indicators including air temperature, precipitation, vegetation coverage and AQI, and 1000 Monte Carlo simulation runs were implemented in total. The atmospheric ecological index was recalculated, and successive zoning reclassification was conducted before the zoning grade shift frequency, and cross-grade transition probability were counted. The zoning coincidence degree and grade retention rate were used as quantitative indicators [38] to judge zoning pattern robustness under different disturbance intensities, and a whole-process robustness test was completed.

2.6. Uncertainty and Reliability Statement

This study identifies three primary sources of uncertainty: First, temporal inconsistency in data. The starting observation time of vegetation coverage (1981) and AQI (2013) is later than that of conventional meteorological indicators, leading to unavoidable missing early data, which has a limited impact on long time-series reconstruction and fitting. Second, factors such as observational data homogeneity, remote sensing inversion errors and changes in site environments cause data uncertainty. Third, the ARIMA model has inherent limitations in characterizing nonlinear processes and extreme fluctuation events, which may affect simulation accuracy for extreme scenarios.

To improve the reliability of this research, all methodological procedures are fully reproducible, and unified standards are implemented for data preprocessing, statistical testing and model parameter configuration. A triple verification system—consisting of cross-validation among multiple stations across seven counties and districts, mutual verification of multiple time-series indicators, and comparison with classical regional studies—is applied to the analysis results to eliminate single-point deviation and guarantee the robustness and regional representativeness of identified spatial patterns and statistical characteristics.

3. Results

3.1. Spatial Distribution Characteristics of Key Atmospheric Ecology Indicators

Based on long-term observational and remote sensing data from 1965 to 2024, the spatial differentiation patterns of six core indicators in Shangluo City were revealed, namely precipitation, NDVI, AQI, temperature, sunshine duration, and relative humidity (Figure 2). Constrained by the mountainous terrain of the eastern section of the Qinling Mountains, precipitation gradually increases from southwest to northeast, with high values concentrated in areas such as Luonan and Shangzhou (Figure 2a), where the forced convergence of water vapor due to terrain uplift is significant. From a spatial perspective, influenced by water and heat conditions as well as altitude gradients, vegetation coverage (NDVI)

shows a pattern of being higher in the southwest and lower in the northeast, with high vegetation coverage areas aligning with high-altitude mountainous regions (Figure 2b). Under the combined influence of human activities and vegetation purification, high AQI values are concentrated in densely populated urban areas such as Shangzhou, Luonan, and Danfeng, while the southeastern region (such as Shangnan) maintains excellent levels (Figure 2c). Affected by the altitude-dependent warming mechanism, temperature shows a significant negative correlation with altitude, with lower-altitude river valleys having higher temperatures and higher-altitude mountainous areas having lower temperatures (Figure 2d). High sunshine duration values are concentrated in the northeastern open river valleys, while the southwestern mountainous areas show low values (Figure 2e). Regulated by the coupling of precipitation and vegetation evapotranspiration, relative humidity shows a pattern of being higher in the southwest and lower in the northeast, which is highly consistent with the spatial differentiation of the NDVI (Figure 2f).

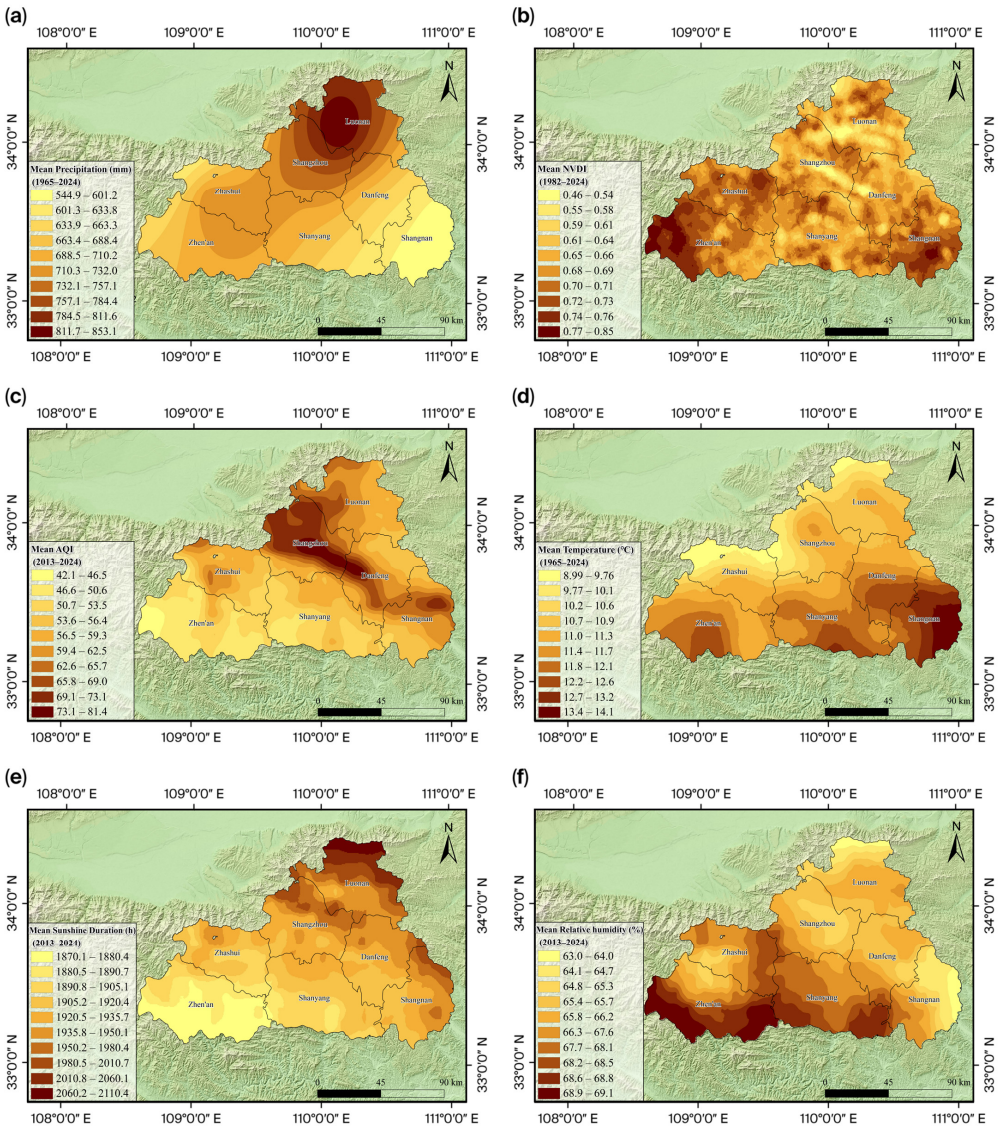

Figure 2. Spatial distribution maps of key atmospheric ecological indicators in Shangluo City, 1965–2024. (**a**) Spatial distribution of precipitation; (**b**) vegetation coverage (NDVI); (**c**) Air Quality Index (AQI); (**d**) air temperature; (**e**) sunshine duration; and (**f**) relative humidity. The national AQI standard was issued in 2012, with official monitoring launched in 2013; vegetation coverage estimation requires NDVI/FVC remote sensing data, with common data sources being GIMMS NDVI (available from 1981 onwards) or MODIS NDVI (available from 2000 onwards) (https://www.resdc.cn). No space-borne vegetation observation data were available internationally before 1981.

3.2. Temporal Evolution and Stationarity Diagnosis of Atmospheric Ecological Indicators

To ensure the scientific validity and reliability of the subsequent ARIMA time-series modeling, this study first analyzed the seasonal evolution characteristics and conducted ADF stationarity tests on the key atmospheric ecological indicators (air temperature, precipitation, relative humidity, sunshine duration, NDVI and AQI) in Shangluo City from 1965 to 2024. Figure 3a clearly illustrates the interdecadal seasonal evolution pattern of air temperature in Shangluo City during the study period: the overall air temperature increased significantly through the decades, exhibiting a temporal differentiation feature of longer warm-season spans and shorter cold-season durations, with a seasonal shift characterized by overall warming. The gray background scatter cloud over the 60-year study period reveals the natural variability in temperature range (−10 °C to 35 °C); the six interdecadal curves show a stepwise upward trend, with the blue curve for the 2010s generally lying above the red curve for the 1960s. Warming is most significant from late spring to early summer, which conforms to the asymmetric pattern of fastest warming in spring (i.e., inconsistent warming rates among seasons). On this basis, quantitative verification of the stationarity of each indicator sequence was performed via the ADF unit root test, and the results are shown in Figure 3b. For the original sequences, the ADF test statistics of temperature, precipitation, and sunshine duration sequences are −1.25, −1.56, and −1.89, respectively, all of which are higher than the 1% significance level critical value of −3.55. The corresponding *p*-values are 0.126, 0.215, and 0.183, all of which are greater than 0.05. Thus, the null hypothesis of a unit root cannot be rejected, and these sequences are determined to be non-stationary (Figure 3b). After first-order differencing of the three sequences, the ADF statistics decreased to −3.82, −3.91, and −3.68, with *p*-values of 0.003, 0.002, and 0.004, respectively. All three sequences passed the 1% significance test and were converted into stationary sequences. For the original sequences of relative humidity and vegetation coverage, the ADF statistics are −2.18 and −2.98, with *p*-values both less than 0.05, indicating that the original sequences are stationary and do not require differencing. Combining the seasonal evolution characteristics and stationarity test results (Figure 3), it can be concluded that all indicator sequences in the study area have stable temporal structures and identifiable interannual variation trends, providing a reliable data foundation for subsequent long-term trend fitting, model optimization and future scenario prediction.

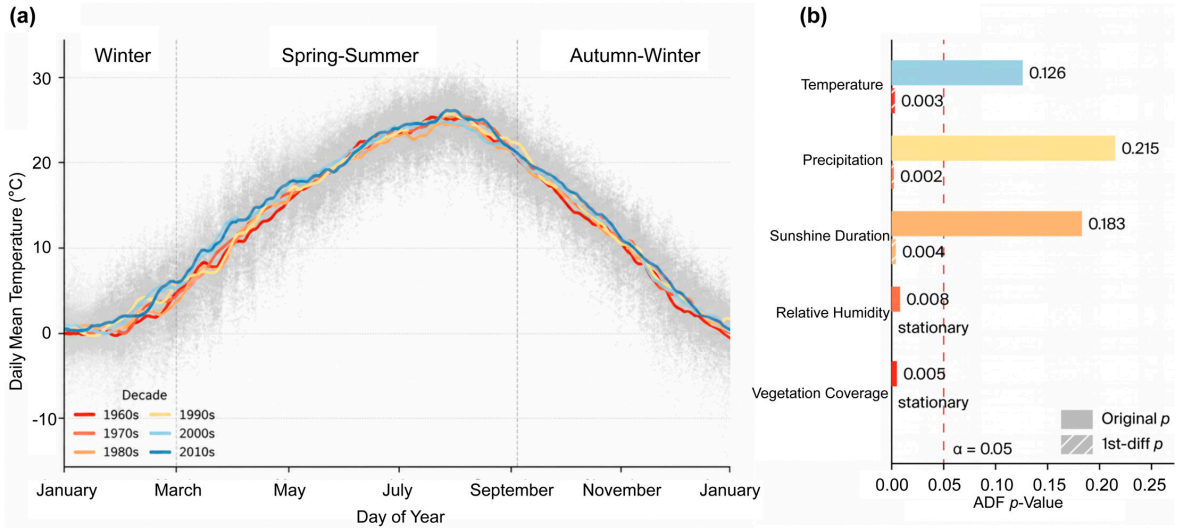

Figure 3. Seasonal variation trajectory of air temperature and ADF stationarity test of time series in Shangluo City (1965–2024). (**a**) Interdecadal seasonal evolution characteristics of air temperature, revealing the shifting pattern of seasonal temperature cycles during the study period; (**b**) Results of ADF stationarity test and first-order difference processing. The vertical dashed line represents the critical value at the 0.05 significance level for judging the significance of ADF test *p*-values.

On the 60-year observational timescale, the annual mean temperature in Shangluo exhibited a persistent increasing decadal trend, with both the median and mean values rising consistently across decades (Figure 4a). The overall dispersion of box plots remained stable, indicating a steady regional warming tendency. A small number of low-temperature outliers were detected in the 1960s and 2010s, reflecting anomalous temperature fluctuations in individual years (Figure 4a).

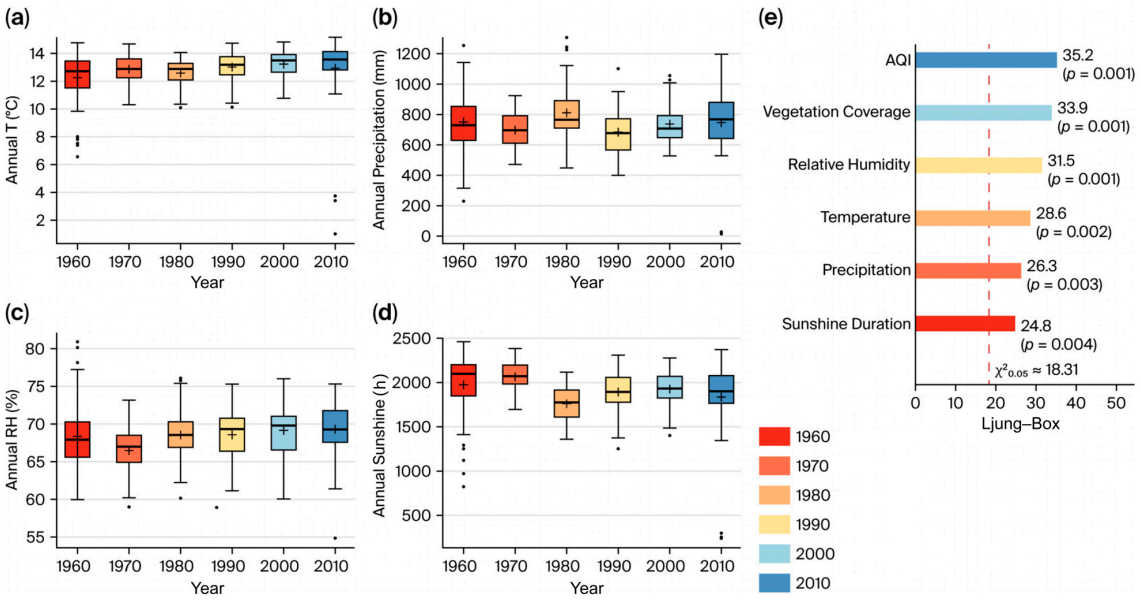

Figure 4. Interdecadal distribution characteristics of multiple meteorological indicators in Shangluo City and Ljung–Box white noise test results (1965–2024). (**a**–**d**) present the interdecadal boxplots of annual average temperature, precipitation, relative humidity and sunshine duration, which demonstrate the central tendency, dispersion degree and outlier variation in each indicator. (**e**) The Ljung–Box Q statistic and its significance level, which verifies the autocorrelation of the sequence and confirms the accuracy of the observations, the vertical dashed line denotes the chi-square critical value of the Ljung–Box test at the significance level $\alpha = 0.05$, which is used to identify significant autocorrelation in time series residuals. This study divided the dataset at a temporal ratio of 7:3 without disrupting the original time sequence from 1965 to 2024. The first 70% (1965–2007) served as the training set, and the remaining 30% (2008–2024) was used as the independent test set. To ensure data sufficiency, the training period was extended to 1960–2010 in the illustration.

Annual precipitation remained relatively stable across decades, with no pronounced long-term increasing or decreasing trends in mean and median values (Figure 4b). Nevertheless, notable differences in interdecadal dispersion were observed; the interannual variability in precipitation was markedly higher in the 1960s, 1980s and 2010s. In particular, extremely low-value outliers emerged in the 2010s, implying that despite an overall stable decadal background of regional hydrological circulation, substantial interannual fluctuations and potential risks of extreme drought and flood events persisted (Figure 4b).

Relative humidity remained at a relatively high level of 65–70% over the long term, with minor fluctuations in decadal mean and median values and insignificant interdecadal discrepancies (Figure 4c). Considerable interannual variability was evident within each decade, collectively providing favorable humidity conditions for regional vegetation growth and atmospheric ecosystem stability (Figure 4c).

Sunshine duration decreased markedly from the 1960s to the 1980s, with the annual mean and median declining from approximately 2050 h to 1780 h. From the 1990s to the 2010s, it fluctuated slightly within the range of 1850–1950 h and tended to be stable overall

(Figure 4d). A small number of extremely low-value outliers appeared in each decade, with particularly pronounced interannual fluctuation amplitudes in the 1960s and 2010s.

The Ljung–Box white noise test demonstrated that the chi-square statistics of all indicators were significantly higher than the critical value ($p < 0.05$), leading to a strict rejection of the null hypothesis of white noise (Figure 4e). This confirms evident autocorrelation structures and extractable time-series information within each dataset, as well as distinct non-random fluctuation characteristics.

Combining the decadal distribution patterns and statistical test results (Figure 4), all seven atmospheric ecological indicators in the study area satisfy three fundamental modeling prerequisites: stationarity, non-white noise characteristics and weak seasonality. These properties guarantee ARIMA model construction reliability and subsequent prediction output accuracy.

3.3. Bivariate Coupling Relationship, ARIMA Model Fitting and Residual Diagnosis

Under the combined influence of regional hydrothermal and topographic radiation patterns, temperature and relative humidity in the study area show a weak positive correlation, with discrete points concentrated in distribution and a clear regression trend (Figure 5a), reflecting the characteristic that humidity increases regularly with rising temperature. Temperature and sunshine duration also exhibit a significant positive correlation (Figure 5b), indicating that radiation and heat conditions form a stable positive coupling mechanism constrained by mountainous topography.

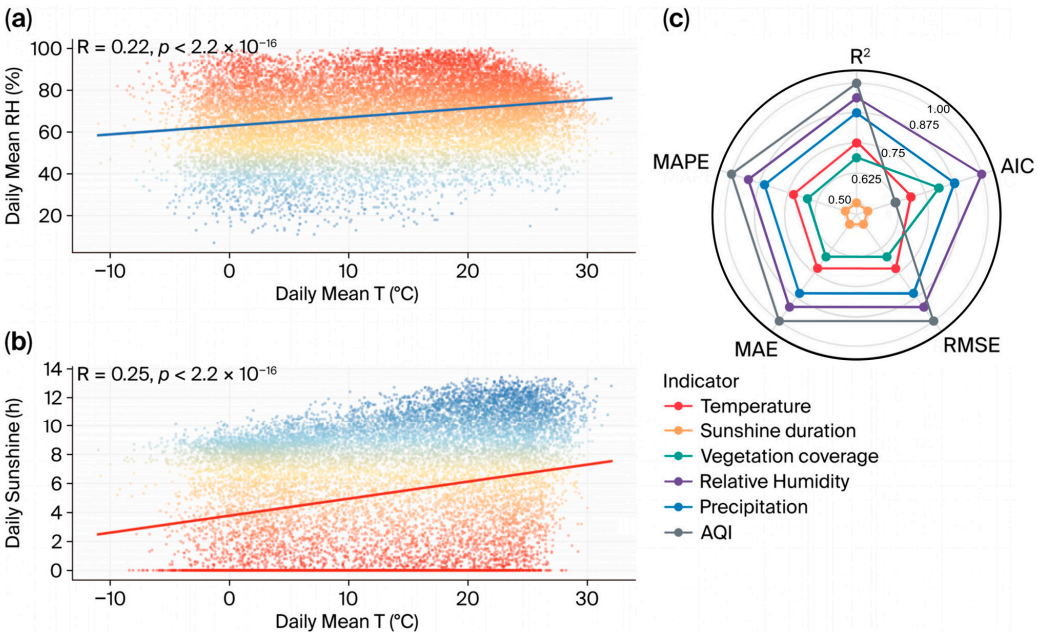

Figure 5. Bivariate coupling relationships of atmospheric indicators and performance evaluation of ARIMA models in Shangluo City (1965–2024). (**a**) The coupling relationship between air temperature and relative humidity.; (**b**) The correlation between air temperature and sunshine duration; (**c**) A standardized radar chart that compares the fitting performance of ARIMA models for each indicator. All numerical values in this figure have undergone within-column min–max rescaling to the range [0.5, 1.0], where 1 indicates that the corresponding indicator achieves optimal performance among the six indicators, thus all axes in the figure are unitless [39]. The R^2 presented in (**c**) is a normalized index, rather than the R^2 of the training set [40].

The standardized radar chart constructed based on Coefficient of Determination (R^2), AIC, Root Mean Square Error (RMSE), Mean Absolute Error (MAE) and Mean Absolute Percentage Error (MAPE) shows that the ARIMA models for all variables demonstrate favor-

able fitting performance (Figure 5c). Among them, the Air Quality Index model has optimal performance across all evaluation indicators, followed by the relative humidity model; the fitting performances for precipitation, temperature and vegetation coverage are generally satisfactory, with only the sunshine duration model being relatively less accurate but still meeting the predictive analysis requirements. Based on the comprehensive model fitting results, the optimized ARIMA models for various atmospheric ecological indicators in the study area have strong applicability, high fitting accuracy and robust structure, which can provide reliable support for subsequent long-term trend simulation and future scenario prediction.

The AIC-based parameter optimization results are as follows: the optimal model for temperature is ARIMA (2,1,1), with AIC = −12.56 and R^2 = 0.89 on the training set, explaining 89% of the temperature variation; the optimal model for precipitation is ARIMA (1,1,1), with AIC = −14.25 and R^2 = 0.91 on the training set, showing a slightly better fitting performance than that of the temperature model; the optimal model for relative humidity is ARIMA (1,0,0), with AIC = −13.89 and R^2 = 0.92 on the training set, exhibiting stable performance; the optimal model for AQI is ARIMA (1,0,0), with AIC = −11.97 and R^2 = 0.94 on the training set, which has excellent performance; the optimal model for vegetation coverage is ARIMA (1,0,0), with AIC = −15.32 and R^2 = 0.95 on the training set, showing the most outstanding fitting performance among all models; and the optimal model for sunshine duration is ARIMA (2,1,2), with AIC = −10.89 and R^2 = 0.85, demonstrating the lowest accuracy among the six models but still remaining at a favorable level. The AIC values of all models are less than −10, and their R^2 values on the training set are greater than 0.85, indicating that they have excellent fitting performance for historical data, as well as a reliable prediction basis (Figure 5c).

The standardized radar chart constructed based on R^2, AIC, RMSE, MAE and MAPE further verifies the model performance: the ARIMA models for all variables all exhibit favorable fitting and prediction performance (Figure 5c). Among them, the AQI model achieves optimal performance across all evaluation indicators, followed by the relative humidity model. The fitting performances of the models for precipitation, temperature and vegetation coverage are generally good; only the accuracy of the sunshine duration model is relatively lower, but it still meets the predictive analysis requirements. Based on the comprehensive model fitting results, the optimized ARIMA models for various atmospheric ecological indicators in the study area have strong applicability, high fitting accuracy and robust structure, which can provide reliable support for subsequent long-term trend simulation and future scenario prediction.

To verify the fitting performance and reliability of the optimized ARIMA model, this study conducts residual diagnostic analysis from three dimensions: normality, independence and homoscedasticity. The Q-Q plot for residual normality shows that the vast majority of sample points closely fit the distribution of the theoretical straight line, with only a slight local deviation at the left tail. Overall, no systematic bias or truncation characteristics are observed, indicating that the residuals follow a normal distribution (Figure 6a). The residual autocorrelation function plot shows that the autocorrelation coefficients at all lag orders fall within the confidence interval, with no significant peaks (Figure 6b), indicating that the residual sequence is mutually independent, the model has fully extracted the temporal information from the original sequence, and no residual autocorrelation structure remains. The vertical axis of this residual sequence plot is set to the range of ±0.2, which is a visual boundary determined based on the actual distribution of residuals (approximately ±0.15) and the 95% confidence interval boundary. This setting not only presents all residual points completely, but also intuitively demonstrates that the residuals do not exceed the theoretical fluctuation range, satisfying the white noise assumption. The residual homoscedasticity test shows that the dispersion degree of residuals remains uni-

formly distributed with the fitted values, and no obvious expansion or contraction trend is observed (Figure 6c), confirming that the model satisfies the homoscedasticity assumption. Based on the comprehensive results of the three diagnostic tests (Figure 6), the optimized ARIMA model fully complies with the statistical assumptions for time-series modeling, with reasonable parameter estimation, stable structure and high fitting accuracy, which can provide reliable support for indicator trend analysis and future scenario prediction.

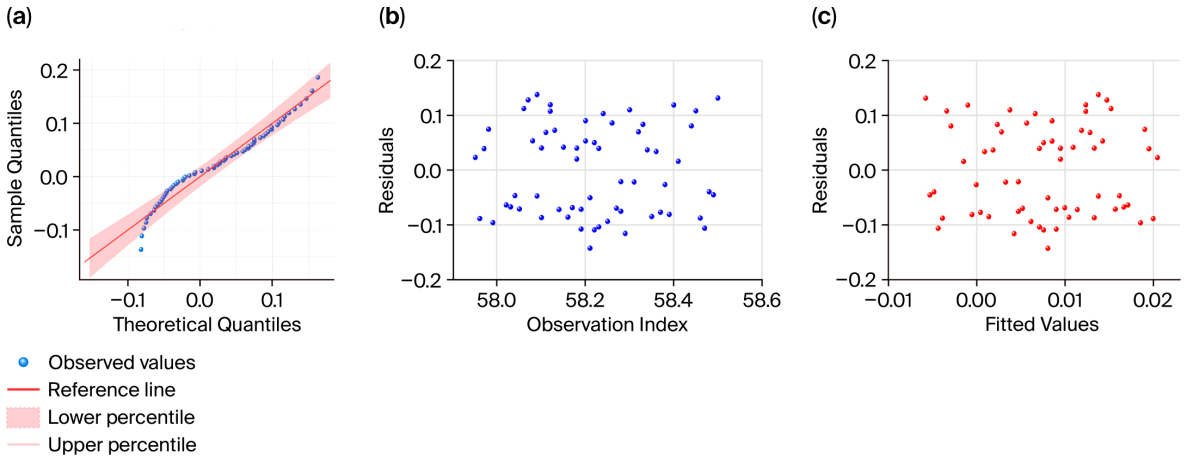

Figure 6. Residual diagnostic plots of the optimal ARIMA model: (**a**) normality Q-Q plot; (**b**) residual sequence (autocorrelation function); (**c**) homogeneity of residuals.

3.4. Decadal Evolution Characteristics of Climate–Vegetation–Air Quality at the County Scale

Based on the ten-year sliding window analysis from 1965 to 2019, Figure 7 systematically reveals the long-term spatial differentiation and decadal evolution patterns of geographical location, annual average temperature, relative humidity, sunshine duration, and total annual precipitation in the seven counties of Shangluo City, clearly presenting the trend characteristics, fluctuation amplitudes, and spatial heterogeneity of each meteorological element at the county scale (Figure 7).

Danfeng County (Figure 7aI) is located in the valley transition zone in the central-eastern part of Shangluo. The unique geomorphological transition attribute endows its interdecadal climate fluctuations with significant phased differentiation characteristics. Interdecadal monitoring results from 1965 to 2019 indicate that the thermal conditions of the county follow a clear phased evolution pattern (Figure 7aII): temperature showed a slightly fluctuating downward trend from 1965 to 1994, and entered a continuous and significant increasing stage after 1995, showing an overall turning change characteristic of decreasing first and then increasing. The above evolution pattern indicates that the closed valley terrain is prone to form a local thermal retention effect, which weakens the regional atmospheric exchange capacity, promotes faster temperature rise in local areas, and thus forms a significant temperature evolution inflection point around 1995. The atmospheric humidity of the county also underwent a dry–wet transition with 1995 as the dividing point (Figure 7aIII). The humidity fluctuated greatly in the early period, and the fluctuation tended to be gentle in the later period, with the local environment gradually developing towards humidification. This indicates that the climate warming inflection point simultaneously changed the local evapotranspiration process and the water vapor budget balance, promoting the transformation of a regional dry–wet pattern from unstable fluctuation to a stable humid state. During the study period, the sunshine resources in the county showed a continuous decreasing trend, and the interdecadal mean value declined steadily (Figure 7aIV). Constrained by the valley terrain on water vapor, regional water vapor input and loss tend to be balanced. Furthermore, precipitation has no significant

increasing or decreasing trend, fluctuating slightly within a stable range all year round, with the hydrological environment remaining stable on the whole (Figure 7aV).

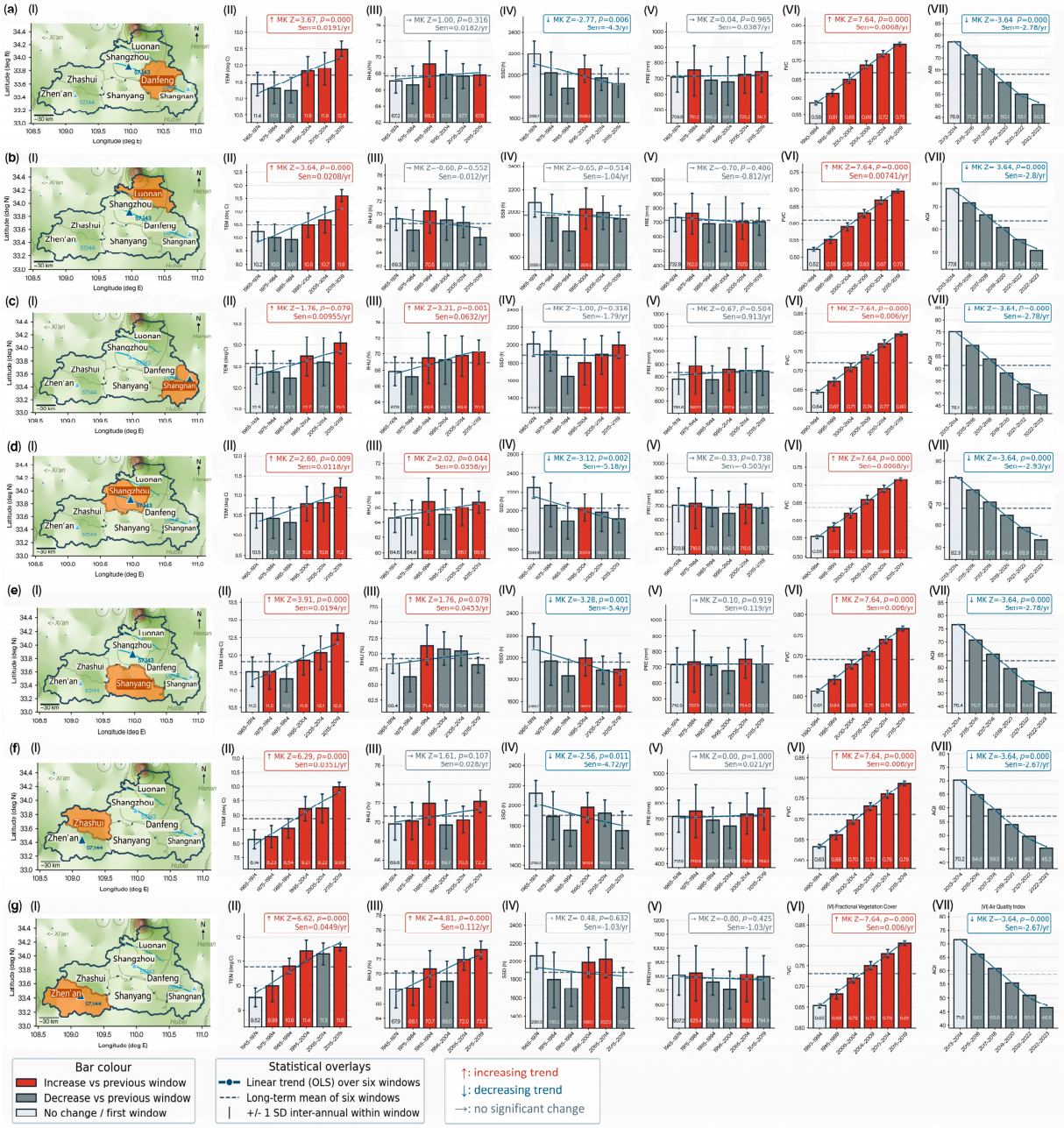

Figure 7. Interdecadal evolution characteristics of multiple ecological and meteorological elements in six counties and one district of Shangluo. Subfigures (**a**–**g**) correspond to Danfeng, Luonan, Shangnan, Shangzhou District, Shanyang, Zhashui, and Zhen'an Counties, respectively. Each subfigure contains seven panels: panel (**I**) illustrates the geographical location of the county, panel (**II**) demonstrates interdecadal variations in annual mean temperature, panel (**III**) exhibits interdecadal variations in relative humidity, panel (**IV**) displays interdecadal variations in sunshine duration, panel (**V**) presents interdecadal variations in total precipitation, panel (**VI**) shows interdecadal variations in vegetation coverage, and panel (**VII**) illustrates the Air Quality Index. Except for vegetation coverage and AQI, all meteorological elements are statistically analyzed over six time windows: 1965–1974, 1975–1984, 1985–1994, 1995–2004, 2005–2014, and 2015–2019. Vegetation coverage is statistically analyzed over six time windows: 1990–1994, 1995–1999, 2000–2004, 2005–2009, 2010–2014, and 2015–2019. AQI is statistically analyzed over six time windows: 2013–2014, 2015–2016, 2017–2018, 2019–2020, 2021–2022, and 2023–2024. Note: MK = Mann–Kendall trend test (alpha = 0.10). Sen = Theil–Sen non-parametric slope. Blue triangles indicate the locations of national meteorological stations.

Luonan County (Figure 7bI) is located in the open basin in the northeast of the study area. Without shielding from high mountains, the flat terrain makes the climate evolution pattern significantly different from that of the southern mountainous areas. The county's temperature evolution has clear levels and prominent phased characteristics (Figure 7bII): it experienced gentle and weak cooling from 1965 to 1994, showing continuous stepwise warming after 1995. This indicates that the open basin in the northeast has better thermal diffusion conditions, responds more directly to regional warming signals, and is more prone to form a stepwise progressive warming process. Different from the increasing humidity trend in most counties in the whole region, the atmospheric humidity of Luonan County shows a fluctuating downward trend, with the local environment becoming drier year by year (Figure 7bIII). The core reason for this contrary humidity decline is that the basin terrain has strong ventilation and that water vapor is easy to dissipate and difficult to accumulate. The open terrain of the basin facilitates smooth atmospheric circulation with relatively less cloud cover. The basin's open terrain allows for smooth atmospheric circulation and relatively low cloud cover. Influenced by local warming-driven atmospheric dispersion, the county has experienced a slight downward fluctuation in sunshine duration over the decades, yet solar resources remain relatively abundant. (Figure 7bIV). During its northward transportation from the southeast monsoon, water vapor gradually decreases. Combined with the guiding effect of the northern terrain on the southward cold advection, the water vapor supply continues to be insufficient, and precipitation shows a weak decreasing trend, making Shangluo a region with low precipitation (Figure 7bV).

Shangnan County (Figure 7cI) is located in the southeastern mountainous area, adjacent to the water vapor input channel, with sufficient supply from the southeast monsoon; as such, the hydrothermal evolution activity is significantly higher than that of other counties. The temperature of the county has maintained a fluctuating warming trend for a long time (Figure 7cII); it decreased slowly in the early period, while the warming rate accelerated significantly after 1995. This indicates that the windward slope of the mountain has abundant water vapor and stronger hydrothermal coupling, which is more likely to amplify the warming amplitude and advance its response rhythm against the background of climate warming. The regional humidity has a superior background and maintains a high level of humidity all year round; the humidity continues to increase on an interdecadal scale, and the humid environment continues to strengthen (Figure 7cIII). This is mainly attributed to the uplift, condensation and retention effects of the windward slope terrain on water vapor, which provides a stable water vapor source for the local high-humidity environment. Affected by the uplift effect of the windward slope terrain, cloud systems form frequently, with dramatic dynamic changes in cloud cover and an obvious time boundary for sunshine. It fluctuated greatly from 1975 to 2014, showing an overall characteristic of variable, slow decline (Figure 7cIV). With continuous and sufficient monsoon water vapor input, combined with the forced uplift of mountain terrain, the county has abundant precipitation with interdecadal fluctuations, and no long-term dry or wet anomaly occurs (Figure 7cV). As such, this provides a sufficient precipitation base for the mountain hydrological system to maintain its own stability and resist interdecadal climate fluctuations.

As the central urban area, Shangzhou District (Figure 7dI) has the transition geomorphology of both the basin and mountain, coupled with disturbance from intensive human activities; as such, the climatic element evolution has an obvious urbanization imprint. Temperature shows a typical two-stage differentiation (Figure 7dII), decreasing weakly in the early period and a prominent warming trend with a clear turning node after 1995. This indicates that the hardening of the urban underlying surface, anthropogenic heat emission, and the heat-gathering effect of the basin significantly amplify the climate

warming signal and strengthen the interdecadal phased turning characteristics of temperature. Affected by the urban heat island effect and hardening of the underlying surface, the regional atmospheric humidity was lower than that of surrounding mountainous areas for a long time. Although it increased slightly on an interdecadal scale, the overall dry pattern remained fundamentally unchanged (Figure 7dIII). The reason is that the proportion of vegetation and water areas in urban locations is low, and the evapotranspiration supply is insufficient, which makes it difficult to reverse the background characteristic of local dryness. Affected by increased aerosol emissions from urbanization, the rising frequency of cloud cover and haze, decreasing atmospheric transparency, and amount of sunshine show continuous fluctuating declines over time with significant interdecadal differences (Figure 7dIV). The basin terrain has a balanced effect on the convergence and regulation of local water vapor, so precipitation shows no significant increasing or decreasing trend and maintains a medium level all year round, making it the region with the most moderate precipitation in the city (Figure 7dV).

Shanyang County (Figure 7eI) is located in the low-to-medium mountainous area in the southern part of the city, where gullies and valleys are densely developed, resulting in complex local microclimates that are highly sensitive to regional climate change. Since 1965, the county's air temperature has shown a continuous and stable increasing trend, with uniform interdecadal growth amplitude and a significant linear warming trend (Figure 7eII). No obvious phased turning point has been observed, reflecting the continuity and stability of thermal response in fragmented mountainous areas. Taking 1984 as a turning point, atmospheric humidity shifted from early-stage fluctuations to a continuous, slight increase in the later period, with the local environment gradually developing towards a more humid condition (Figure 7eIII). Affected by the increase in cloud cover, against the background of regional warming and frequent local foggy weather, and combined with the significant shading effect of the mountains, the reduction amplitude of annual sunshine duration in the county ranks first among all counties in the southern mountainous area, showing a clear interdecadal decreasing trend (Figure 7eIV). The regional precipitation has a high base level with gentle inter-annual fluctuations, and no observed extreme alternation between wet and dry periods (Figure 7eV). This is mainly attributed to the interception, retention and redistribution of water vapor by undulating mountains, ensuring stable precipitation recharge and strong anti-disturbance in the regional hydrological system.

Zhashui County (Figure 7fI) is located in the high-altitude core area of the Qinling Mountains in the southwest of Shangluo, with an overall high terrain and continuous mountain ranges. Altitude differences dominate the evolution process of the local climate. From 1965 to 2019, the county's air temperature showed a continuous and steady upward trend, with a continuous and persistent warming process (Figure 7fII). Due to the clean and transparent atmosphere in high-altitude areas and the more sensitive thermal feedback of the underlying surface, these areas' degree of response degree to regional climate warming is significantly higher than that of low-altitude areas, showing a remarkable warming amplification effect. Affected by the strong interception of water vapor carried by the southeast monsoon by the Qinling Mountains, as well as the frequent formation of local fog, the overall atmospheric humidity in the county has remained at the highest level in the whole city for a long time, showing a continuous fluctuating upward interdecadal trend and forming a stable high-humidity environment (Figure 7fIII). Influenced by the prominent shading effect of high-altitude mountains and the reduced atmospheric light transmittance caused by perennial foggy weather, the baseline of sunshine duration in the county was generally low during the study period, showing an inter-decadal fluctuating downward trend (Figure 7fIV). The tall mountains effectively block and retain water vapor, resulting in abundant total precipitation resources with weak interdecadal fluctuations

and long-term stable hydrological conditions, firmly guaranteeing continuous regional ecosystem improvement (Figure 7fV).

Zhen'an County (Figure 7gI) is located in the medium-high mountainous area in the southwest of Shangluo; together with Zhashui County, it forms a continuous Qinling mountain ecological barrier. The regional climate evolution has strong spatial consistency and integrity. The overall air temperature in the county shows stable warming, with no obvious cooling fluctuation period; as such, the high-altitude terrain's warming amplification effect is clearly presented (Figure 7gII). Water vapor in the region is continuously intercepted by continuous mountains, meaning atmospheric humidity has remained at a high and stable level for a long time, with extremely small interdecadal fluctuation amplitude and strong humid environment stability (Figure 7gIII). Jointly affected by the shading of continuous mountains and perennial foggy weather, atmospheric transmittance has continued to decrease, resulting in weak baseline light conditions, with sunshine resources showing a significant fluctuating downward trend (Figure 7gIV). The continuous tall mountains in the southwest form a stable water vapor retention area, leading to sustained and sufficient precipitation recharge and gentle interdecadal evolution, with no drastic dry–wet abrupt changes (Figure 7gV). The hydrological system is less disturbed by external climate fluctuations, with outstanding self-regulation and anti-disturbance capabilities.

On the whole, with the evolution of climate elements, vegetation coverage in all counties has increased year by year after 1990, showing a clear trend of ecological improvement (Figure 7a–gVI); air quality showed obvious improvement after 2013 (Figure 7a–gVII). This indicates that the climate combination of overall warming, increasing humidity and stable precipitation has significantly optimized the regional hydrothermal matching conditions, reduced the inhibitory effect of climate stress on vegetation growth, and created a favorable climatic environment for continuous vegetation restoration. The steady increase in vegetation coverage further enhances the capacity of surface dust retention, water vapor regulation and local atmospheric purification; effectively reduces atmospheric pollutant accumulation; and promotes simultaneous air quality improvement. The steady evolution of climate elements and continuous ecosystem optimization has formed positive feedback, which jointly reflects the fact that the atmospheric ecosystem of Shangluo mountainous areas tends to be stable, as well as that the overall anti-disturbance and self-regulation capacities have been continuously enhanced. The interdecadal evolution of meteorological elements in counties of Shangluo City presents an overall pattern of widespread warming across the region, increasing humidity (except Luonan), slow decline in sunshine (except Luonan), and decreasing precipitation (except Luonan). Spatially speaking, the counties in the southwest (Zhashui, Zhen'an) have higher humidity, more abundant precipitation and lower sunshine; the basins in the northeast (Luonan, Shangzhou) have higher air temperature, lower humidity and more sunshine. No extreme abrupt changes occurred in each element from 1965 to 2019, and the interdecadal trend was stable, which provided a stable climate background for the atmospheric ecosystem that was highly coupled with the subsequent hierarchical and zoning pattern of the atmospheric ecological index.

3.5. Atmospheric Ecological Index Prediction from 2025 to 2040 and Zoning Robustness Test

Based on the prediction of the ARIMA model and the synthesis of the AEI through AHP expert weighting, we first analyzed the statistical characteristics of the original observational data regarding the key meteorological driving factors in the seven districts and counties of Shangluo City. Figure 8a shows that the daily temperature observations at each station present a typical bimodal distribution, with peaks concentrated in the 0–5 °C and 15–25 °C intervals, reflecting the seasonal differentiation of winter and summer temperatures in the study area. Moreover, the different stations' distribution curves are

highly similar, indicating the weak spatial heterogeneity of regional temperatures. Figure 8b shows the kernel density distribution of daily relative humidity at each station, which is generally unimodal and skewed, with the peak concentrated in the 60–80% interval. The distribution of sunshine duration in Figure 8c shows a clear bimodal structure, with short (0–4 h) and long (8–12 h) periods being high-frequency intervals. The curve shapes of different stations are almost identical, indicating that the influence of terrain shading on sunshine duration in the study area is uniformly bimodal, with no significant regional differences. The daily precipitation distribution in Figure 8d shows a highly right-skewed L-shaped distribution, with the majority of daily precipitation being less than 10 mm and the frequency of extreme precipitation events being extremely low. The distribution curves of different stations almost overlap, indicating strong regional consistency in precipitation.

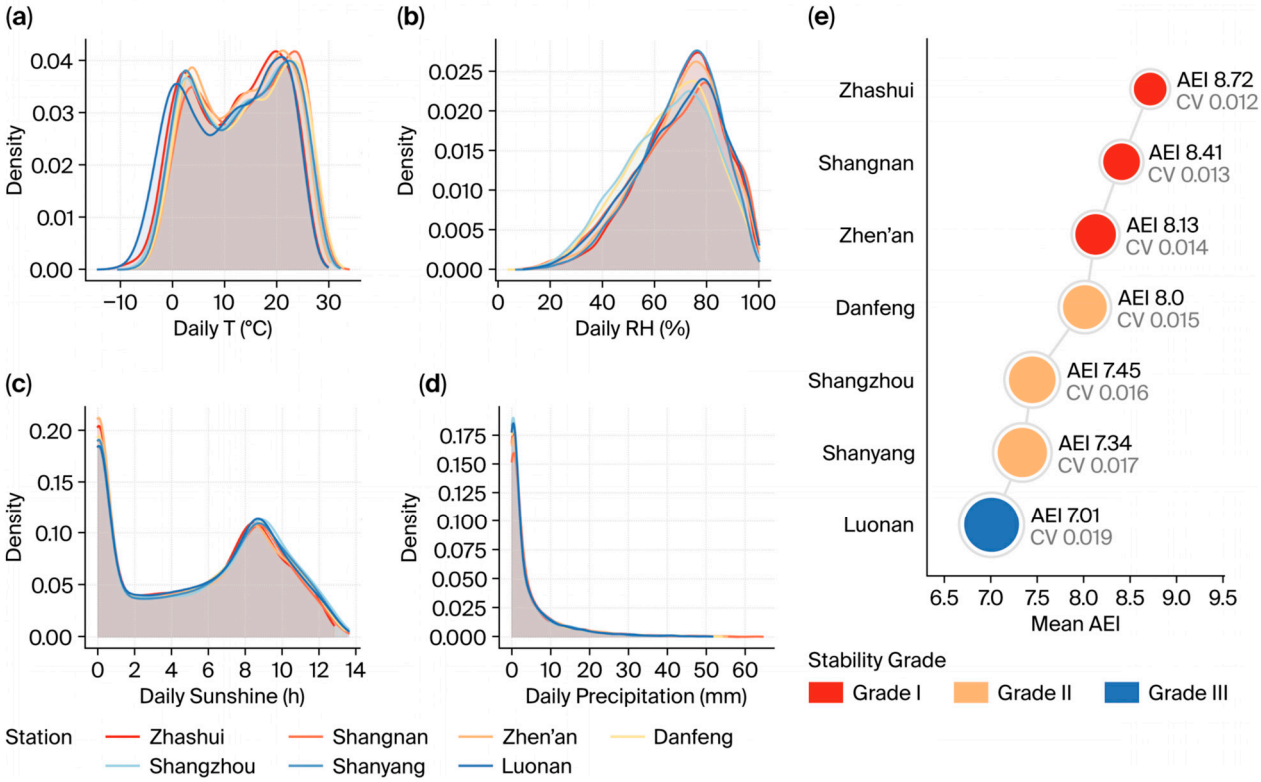

Figure 8. Density distribution of site-level raw observational data and regional atmospheric ecological index (AEI) grading evaluation. (**a**) Kernel density distributions of daily average temperature; (**b**) relative humidity; (**c**) sunshine duration; (**d**) and daily precipitation observational data at each site. (**e**) Mean, coefficient of variation (CV), and stability grading of regional AEI at each site.

Based on this, the regional AEI classification results (Figure 8e) show that Zhashui (AEI = 8.72, CV = 0.012), Shangnan (AEI = 8.41, CV = 0.013), and Zhen'an Counties (AEI = 8.13, CV = 0.014) are classified as Grade I, excellent areas (AEI > 8.0); Danfeng County (AEI = 8.00, CV = 0.015), Shangzhou District (AEI = 7.45, CV = 0.016), and Shanyang County (AEI = 7.34, CV = 0.017) are classified as Grade II, good areas ($7.0 < AEI \leq 8.0$); and Luonan County (AEI = 7.01, CV = 0.019) is classified as a Grade III, medium area ($6.0 < AEI \leq 7.0$). Moreover, the coefficient of variation in each district and county is less than 0.02, and there is no significant numerical fluctuation, indicating that the AEI has extremely high stability at the station scale.

4. Discussion

Based on the continuous 65-year ground observation sequence from 1965 to 2024 in Shangluo City, in the eastern section of the Qinling Mountains, this study constructed a

multi-dimensional diagnostic–time-series prediction–dynamic zoning integrated assessment system, systematically revealing the long-term evolution characteristics, multi-factor coupling mechanisms, spatial differentiation patterns, and future stability paths of the atmospheric ecosystem in ecologically fragile mountainous areas. The research results have broken through the limitations of traditional static assessments in depicting long-term trends, including the insufficient quantification of synergy effects and a lack of robustness tests for zoning results at the county scale. This has deepened our understanding of the climate–ecosystem evolution mechanism in the Qinling Mountains and can provide a basis for ecological protection and climate adaptation decision-making in the Qinba Mountain Area, as well as a replicable and transferable paradigm reference for global similar mountainous ecosystem research.

4.1. Regional Characteristics, Global Commonality, and Driving Mechanism of Altitude-Dependent Warming

The atmospheric ecological indicators in the study area show a long-term steady-state evolution pattern of "three stabilities, three gradual changes, and one optimization", breaking the common perception of the Qinling Mountains as being "highly vulnerable and highly sensitive" [41]. The core driving force stems from the synergistic positive effect of long-term ecological protection policies and the natural self-regulation mechanism of the mountainous area. From 1965 to 2024, the study area's temperature exhibited a significant Elevation–Dependent Warming Enhancement (EDWE) [42,43]. The high-altitude counties in the eastern section of the Qinling main ridge, such as Zhashui and Zhen'an (average altitude > 1100 m), are dominated by deep canyons and mid-high mountains, with high terrain enclosure, weak atmospheric ventilation and diffusion conditions, stable surface net radiation input, and weak human activity disturbance, maintaining a high vegetation coverage rate for a long time. These areas have become typical climate-sensitive response units in the high-altitude rocky mountainous areas of the eastern Qinling Mountains [44]; driven by the coupling of topography, atmospheric radiation, and local circulation [45], their warming rate is significantly higher than that of the low-altitude river valleys and basins such as Luonan and Shangzhou, ultimately forming a spatial differentiation pattern where temperature increase is highly coupled with the altitude gradient.

The Elevation–Dependent Warming (EDW) pattern identified in this study is highly consistent with the global observations of mid-latitude mountainous systems, highlighting its cross-regional universality. Pepin et al. [46] found that warming in the mid-latitude mountainous systems is not uniform across the entire region but follows a vertical mode of "strongest warming at the snow line/vegetation transition zone and a deceleration of warming at extremely high altitudes". The EDW signal in the Qilian Mountains is relatively weak [46,47], the warming peak in the Nyainqentanglha Mountains is at 4500–5500 m [46], and warming above 6000 m in the Himalayas has stagnated or even cooled locally [46], which is consistent with the spatial pattern of stronger warming in the high-altitude southwest and milder warming in the low-altitude northeast. Long-term meteorological observations and terrain numerical simulations in the European Alps and the North American Rocky Mountains also confirm [48] that the warming rate in the 1000–2500 m mid-high altitude zone can be 1.5 to 2 times that of the low-altitude basins, and the topographic thermal trap effect formed by closed valleys easily intensifies the accumulation of near-surface heat, which is highly consistent with the terrain-driven warming characteristics of the high-altitude counties of Zhashui and Zhen'an. Long-term monitoring results in the Scandinavian Mountains further confirm that accelerated warming at high altitudes in mid-latitude mountains is a global commonality [49].

Combining an understanding of the global mountain mechanism with the regional characteristics of this study, the intrinsic driving mechanism of EDW in the study area can be

summarized into three synergistic paths, all of which are homologous to the mechanisms of typical mid-latitude mountains. The first is the altitude-differentiated effect of radiative forcing: the atmospheric column at high altitudes is thinner, and the aerosol load is lower, and the increase in greenhouse gases leads to a more significant increase in downward long-wave radiation, which directly contributes to near-surface warming [50] and lays the physical foundation for regional climate thermal buffering. The second is the surface–atmosphere feedback amplification effect: the melting of high-altitude snow and the change in the phenological rhythm of vegetation jointly reduce the surface albedo, enhance the ability to capture solar radiation, and form a positive feedback loop of "temperature rise–albedo reduction–further temperature increase". This mechanism is highly consistent with the warming intensification mechanism near the snow line on the Qinghai–Xizang Plateau [46,51], which proposes the daytime warming feature in the 3500–5000 m snow line zone, confirming that the surface cover type (snow/vegetation) is the core controlling factor regulating the vertical temperature increase structure in mountainous areas; at the same time, high-coverage vegetation can cooperate with the terrain to lift the latent heat flux and suppress the near-surface sensible heat warming, jointly participating in mountain climate buffering and regulation. The third is the topographic thermal trap effect: the composite landform of mountainous plateaus and canyons in the eastern section of the Qinling Mountains hinders the horizontal diffusion of heat, while the superimposition of the heat convergence effect of the local valley wind circulation intensifies the near-surface heat retention and accumulation [52], thereby amplifying the regional EDW response intensity.

There is a very strong negative correlation between regional elevation and temperature ($r = -0.89$), which directly confirms that high-altitude terrain has a significant climate thermal buffering effect and can effectively mitigate extreme abnormal warming. This buffering process is intrinsically related to the physical mechanism of the deceleration of warming in the extremely high-altitude areas of the Qinghai–Xizang Plateau [53]. Under the joint regulation of radiation, vegetation, and terrain, it not only explains the long-term stable spatial pattern of the atmospheric ecological index in Shangluo City, which is "high in the southwest and low in the northeast", but also provides cross-mountain theoretical support for ecologically sensitive mountainous areas to enhance climate resilience through the joint conservation of terrain and vegetation restoration.

The high robustness of the atmospheric ecosystem in the study area has been verified by both methodological and long-term predictions. It resonates with the long-term evolution laws of European mountains [7], highlighting the global reference value of the research. The long-term research consensus in European mountains clearly states that long-term continuous dynamic monitoring can more accurately depict the ecological resilience of mountains than static cross-sectional assessment. Weak seasonal fluctuations and low coefficient of variation are the core indicators of high ecosystem robustness [54], which is highly consistent with the integrated dynamic assessment framework and ARIMA model prediction results (the coefficient of variation in the regional ecological index is less than 0.03) in this study, highlighting the innovative advantages of the research methodology over traditional static evaluation systems. Future 15-year climate scenario projections show that there will be no grade-level jumps in the ecological zones of the study area, and that the coefficient of variation will remain within 0.03, which is consistent with the robustness of the ecological zones in European mountains under RCP climate scenarios [55]. In the Taihang Mountain gradient study, under moderate climate disturbances, the mountain ecological grades show only small fluctuations in the index without structural jumps [56], which is mutually confirmed by the Monte Carlo simulation results of this study, demonstrating that high-intensity ecological protection can significantly enhance the resilience of sensitive mountains to climate disturbances.

Compared with existing regional studies, this study has achieved an innovative scale-down in the identification and mechanism analysis of EDW. Existing studies on the Qinba Mountains mostly focus on the vegetation's macro-scale response to climate. Chen Chaonan et al. (2019) relied on multi-source NDVI datasets such as GIMMS, SPOT-VGT, and MODIS to reveal that the vertical differentiation law of high-altitude vegetation is more sensitive to temperature, while low-altitude vegetation is more sensitive to precipitation in an area of approximately 300,000 km^2 [57]. Based on MODIS LAI, LST, and TVDI data, Dong Qingdong et al. (2023) confirmed that the greenness of vegetation in the Qinba Mountains first increases and then decreases with altitude, and the surface thermal and soil moisture are significantly differentiated due to terrain redistribution [58]. This study, however, delves into a more detailed scale at the county level. By conducting a local comparison between the high-altitude counties of Zhashui and Zhen'an and the low-altitude basin counties of Luonan and Shangzhou, we have clarified that warming amplification in mountainous areas is not a uniform regional trend, but rather a local intensification phenomenon dominated by high-altitude counties and strongly regulated by canyon topography. This effectively addresses the deficiency of coarse-scale studies in depicting the spatial heterogeneity of warming in mountainous areas and enriches our understanding of the spatial pattern and multi-factor driving mechanism of EDW in the Qinba Mountains at the county level.

4.2. Stability, Robustness and Regional Distinctiveness of Atmospheric Ecosystems

Different from the significant upward trend observed in regional temperature, this study demonstrates that annual precipitation and sunshine duration in Shangluo and the Qinling-Daba Mountains exhibit a gentle and slow declining trend, with no significant abrupt changes or extreme deviations, indicating that the overall hydrometeorological system in the study area possesses strong self-stability and buffering capacity. This characteristic contrasts sharply with the dramatic response pattern observed in the European Alps and Scandinavian Mountains against the background of climate warming, which is characterized by sharp reductions in snow cover, rapid glacier retreat and continuous permafrost warming. Under the combined effects of topographic barriers and vegetation and monsoon regulation, the stability of the hydrothermal system in mid-latitude transitional zone mountains is significantly higher than that of sensitive cryospheric regions in Europe [59]. Meanwhile, Beniston et al. (2018) [48] also confirmed that indicators such as relative humidity, vegetation coverage and Air Quality Index in European mountains have remained stable for a long time (vegetation coverage stays at 68–88%, and AQI stabilizes in the excellent range of 50–65), which verifies the long-term effectiveness of ecological protection and vegetation restoration. This finding is highly consistent with the rule obtained in this study that vegetation in high-altitude areas is more sensitive to temperature, and also aligns with the core conclusion of European mountain research that "high vegetation coverage can mitigate climate stress through albedo regulation, soil water retention and slope stabilization".

Further results from the STL seasonal decomposition conducted in this study show that the overall atmospheric ecosystem in the study area is characterized by weak seasonality and strong interannual variation, with low seasonal fluctuation amplitude, which effectively reduces periodic interference in time-series analysis and improves the reliability of long-term trend identification. This characteristic is similar to the evolution law of cryospheric indicators in European mountains, which is dominated by small seasonal amplitude and interannual variability [60]. However, due to the monsoon climate and dense vegetation coverage in the study region, the seasonal signal is weaker, and the system is more stable, which is also an important distinguishing sign from the strong seasonal fluctuation of

snow cover–permafrost in high-altitude European mountain areas [60]. In conclusion, high vegetation coverage acts as the core regulating factor and, combined with the topographic thermal buffering effect and weak seasonality, jointly constitutes the internal mechanism of high robustness and low sensitivity of the atmospheric ecosystem in the study area, enabling it to maintain a relatively stable hydrothermal and ecological pattern against the background of climate warming [61], which also explains the core reason for the strong self-stability of the hydrometeorological system in the study area.

The zonal results of the atmospheric ecological index obtained in this study, after double verification by coefficient of variation and Monte Carlo simulation, exhibit extremely strong stability and anti-disturbance ability, which makes up for the defect that most zonal studies ignore extreme climate scenarios. During the forecast period from 2026 to 2040, the AEI coefficient of variation in all counties is less than 0.03, reaching a highly stable level; Zhashui County has optimal stability, while Luonan County has a relatively higher coefficient of variation but is still far below the threshold. The results from 1000 Monte Carlo simulations show that even under the extreme scenario of accelerated warming and reduced precipitation, no grade transition occurs in all counties. The first- and third-grade zones remain completely stable, and only small fluctuations are observed in the second-grade zone, confirming that the zonal results have strong robustness.

Spatially speaking, AEI presents a stable pattern of being high in the southwest and slightly low in the northeast. This pattern is highly consistent with the vegetation greenness pattern of the Qinling-Daba Mountains, as revealed by Dong et al. (2023) (the south slope outperforms the north slope, and high-altitude areas outperform low-altitude areas) [58]. The pattern is also highly coupled with altitude, vegetation coverage and human activity intensity: high-altitude areas with high vegetation coverage, such as Zhashui, Zhen'an and Shangnan, are stably classified as first-grade excellent zones; urban agglomeration areas such as Shangzhou, Danfeng and Shanyang are classified as second-grade good zones; and Luonan is classified as third-grade medium zone due to its high topographic openness and relatively weak vegetation advantage. The internal mechanism is that topography and vegetation jointly form a systematic buffer, with strong synergy among multiple factors, so external disturbances can hardly break through the grade threshold. This is highly consistent with the "five-body collaborative evolution of forest–soil–rock–mountain–water" theory proposed by Peng et al. (2023) [62], which clarifies that the Qinling ecosystem has strong self-healing and anti-interference abilities, providing solid theoretical support for the zonal stability obtained in this study.

In conclusion, while this region exhibits the temperature increase response characteristics common to global mountains, it also shows much lower hydrothermal fluctuation and ecological disturbance intensity than European mountains due to its unique location in the north–south transitional zone, topographic barrier, high vegetation coverage and ecological protection effectiveness [1], reflecting the unique advantages and stability mechanism of mountain ecosystems in China's north–south transitional zone in climate adaptation. This further confirms that, in mountain ecosystems, the high-altitude thermal buffering effect, the synergistic gain of vegetation and air quality, and the enhanced stability in low human disturbance areas are natural laws that generally exist across regions [56,63].

4.3. Four-Dimensional Coupling Mechanism and Synergistic Benefits of Topography–Climate–Vegetation–Air Quality

This study quantitatively reveals the stable and synergistic relationship of the four-dimensional coupling of topography–climate–vegetation–air quality in the eastern section of the Qinling Mountains, constructing a closed-loop gain mechanism of "topography regulating climate, vegetation purifying air, climate adapting to vegetation, and air feedback to the ecosystem". By combining mountain vertical zonation and cross-border ecological

comparison, the internal mechanism of multi-factor feedback is further clarified, which can provide a cross-scale theoretical reference for the trade-off of mountain ecosystem services, the maintenance of ecological integrity, and the spatiotemporal correlation laws of climate and vegetation.

Based on ecological assessment and ecological geological theory, He et al. (2023) proposed the "reference system–current status–change" framework, emphasizing that the integrity of ecosystem structure and function is the core for maintaining a stable ecosystem service supply [64]. The 60-year long-term ecological indicators in this study area show weak seasonality and low interannual fluctuations, confirming the basic attribute that a complete ecosystem has strong resistance and resilience. Relying on the differences in regional natural endowments, this study identified significant synergistic relationships between altitude and temperature ($r = -0.89$), and vegetation coverage and air quality ($r = -0.76$), presenting a unique coupling pattern specific to mountainous areas, indicating that the multi-factor feedback pattern is strictly constrained by the natural topography-dominated differentiation. At the same time, high-altitude landforms form a significant thermal buffering effect through energy redistribution, effectively alleviating local abnormal warming against the background of regional warming. This physical regulation process is highly consistent with the academic viewpoint of Peng et al. (2023) that "geomorphology is an ecological container and topography is an ecological regulation carrier" [62], jointly constituting the theoretical basis and geomorphic physical premise of the four-dimensional coupling pattern.

Cross-mountain range comparative analysis further reveals the universal laws of ecological coupling in mid-latitude mountains and the regional particularity of the eastern section of the Qinling Mountains. In their study of Gaoligong Mountain, Yang et al. (2025) [65] confirmed that the altitude gradient is the dominant factor in the ecological service synergy pattern, and the mid-altitude broad-leaved forest belt is more likely to form a synergy peak of carbon storage and habitat quality. This gradient law is consistent with the evolution path of the eastern section of the Qinling Mountains, where topography inhibits warming, improving vegetation growth and the atmospheric environment, confirming that the mid-altitude is the key interval for the mountain topography–climate–vegetation synergy evolution. Combining the quantitative correlation between vegetation, air quality, dust retention, particulate matter adsorption, and boundary layer regulation, as well as the mechanism proposed by Zhai et al. (2022) [66], this study further extends the ecological effects of vegetation from traditional ecological service synergy to the dimension of atmospheric environment purification, improving the comprehensive gain path of mountain vegetation "carbon sequestration–greening–air purification". European mountain research also points out that topography–vegetation–climate can form a stable negative feedback system, maintaining the water and heat balance and the ecological stability of the underlying surface through the cooling effect of high altitudes and high vegetation coverage [48], indicating that the four-dimensional coupling characteristics of the eastern section of the Qinling Mountains are not a local exception but a common ecological resilience mechanism in mid-latitude mountains. The internal energy balance, hydrological buffering, and geomorphic stability processes are highly consistent with the conclusions of this study. In summary, topography constitutes the basis of the four-dimensional coupling, vegetation determines the intensity of synergistic benefits, climate plays the role of connecting and modulating elements, and air quality directly reflects the ecological synergy effect. The four elements form an inseparable organic feedback system under the constraint of vertical gradients. Guo (2024) demonstrated through time-series analysis based on CNN-LSTM deep learning that there are significant nonlinear spatiotemporal correlations between climate factors such as temperature, precipitation, humidity, vegetation and the atmospheric

environment [67]. This finding supports the robust weak correlations between climate elements, relative humidity and sunshine duration in this study, indirectly explaining the intrinsic connection between vegetation and air quality patterns and clarifying the pivotal role of climate in the four-dimensional mutual feedback system. Under the continuous modulation of topography and landforms, the multi-factor correlations in mountainous areas exhibit typical nonlinear evolution characteristics, which can explain the long-term robustness of the coupling relationship in this study without trend reversal or intensity attenuation over 60 years of observation and the next 15 years of prediction. It also reasonably explains the vertical differentiation law that "high altitudes are not optimal for synergy, while mid-altitudes form the peak of synergy". Compared with previous studies that were mostly limited to single-factor or bivariate correlation analysis, this study extends the mutual feedback mechanism to a four-dimensional quantitative analysis framework of terrain–climate–vegetation–air quality, enriching and supplementing the connotation and regional applicability of the coupling theory of the ecosystem in the Qinba Mountain Area. The eastern section of the Qinling Mountains is located in the transitional zone between the north and south climates, with a steep water and heat gradient, significant terrain barrier effects, and high vegetation coverage continuity [68], which has created a stronger four-dimensional coupling association and higher system stability, gradually developing into a dual ecological barrier function of climate regulation and air purification. Overall, the study area shows the evolution characteristics of synergy dominance, weak trade-offs, and high robustness, constituting a typical steady-state case formed under the joint action of the natural background constraints of mountainous areas and long-term ecological protection.

4.4. Methodological Contributions of the Integrated Framework and ARIMA Model Optimization

This study constructs a multi-dimensional diagnosis–time-series prediction–dynamic zoning integrated assessment system. At the time-series diagnosis level, a four-level quality control framework is established, including an ADF stationarity test, Ljung–Box white noise test, STL seasonal decomposition, and residual normality test. Compared with the limitations of Silva et al.'s study (2021), which only used a single ADF to identify time-series signals [69], this study effectively eliminates random noise in the sequence and avoids the risk of spurious regression through multi-step stepwise verification, accurately identifying the true evolution trend of weakly fluctuating and slowly changing atmospheric–ecological sequences, which is suitable for the nonlinear and non-stationary complex characteristics commonly found in mountain climate and ecological time series.

In the prediction modeling stage, this study uses grid search combined with information criteria to optimize the ARIMA model parameters and introduces physical prior constraints such as terrain and vegetation as the underlying surface, balancing data-driven fitting accuracy and the physical interpretability of mountain ecological processes. The R^2 of the model training set is between 0.85 and 0.94, and the MAPE of the test set is less than 1.5%. The prediction performance is significantly better than that of pure machine learning black box models without physical mechanism constraints. This modeling concept is highly consistent with the core view proposed by Tebaldi et al. (2021) that long-term climate and ecological predictions based on the CMIP6 multi-model ensemble need to simultaneously consider physical constraints and model stability [70], highlighting the scientific and universal nature of the model architecture design in this study.

The synthesis of ecological indices adopts AHP expert scoring combined with weighting, and consistency checks are conducted to ensure the objectivity and reliability of the weight distribution. Sun et al. (2019) confirmed that the integration of subjective and objective weighting combined with time-series trend prediction is a key technical path for refined ecological evaluation in mountainous areas, and their research paradigm is highly

consistent with the technical logic of AHP expert weighting coupled with ARIMA model optimization in this study [71]. This further indicates that the combination of subjective and objective weighting and fine parameter optimization is a universal core paradigm for quantitative mountain ecology assessment.

From a methodological comparison perspective, Gong et al. (2024) constructed a CNN-LSTM hybrid model, relying on the convolution module to extract spatial features and LSTM to capture temporal dependencies [72], outperforming single neural network structures in climate element fitting. In this study, the idea of spatiotemporal fusion modeling to adapt to complex mountain environments complements the strategy of embedding terrain spatial priors into time-series modeling: although the model architectures are different, both emphasize the need to fully incorporate the spatial heterogeneity constraints of the underlying surface in mountain ecological prediction, providing two parallel technical paths of statistical time series and deep learning for long-term ecological prediction in mountainous areas, enriching the method selection system for similar mountain time-series modeling.

Different from the traditional static cross-sectional assessment that can only depict instantaneous ecological states, and from the conventional single-time-series model that lacks full-process quality control and robustness verification [12], the integrated framework in this study has the ability to quantitatively predict medium- and long-term evolution trends, achieving a full-chain closed-loop integration of diagnosis–modeling–prediction–zoning–robustness verification. The method has stronger repeatability and regional transferability, effectively filling the methodological gap of the lack of long-term dynamic integrated assessment paradigms in ecologically fragile mountainous areas.

4.5. Limitations and Future Work

Although this study has constructed a relatively complete atmospheric ecological assessment framework based on 60 years of long-term data, there are still inherent limitations in data acquisition and method design when conducting long-term dynamic assessment in ecologically sensitive mountainous areas.

First, the observation time series of core indicators is not uniform. The Normalized Difference Vegetation Index and Air Quality Index started to be observed relatively late, inevitably introducing systematic biases. Such data constraints limit the precise matching and attribution analysis of high-frequency and short-cycle ecological fluctuation events. Secondly, the atmospheric ecological index is influenced by the coupling and interaction of multiple factors such as temperature, precipitation, vegetation coverage, and air quality, making it difficult to quantitatively isolate the independent contribution of a single factor. In areas with stable precipitation and weak human disturbance, the ecological evolution trend is mainly influenced by natural climate variability; conversely, local pollutant emissions, land use changes, and other intense human activities significantly increase driving attribution uncertainty. Although the overall ecological evolution in the study area is mainly driven by natural forces, local human disturbances still reduce the accuracy of the driving mechanism analysis.

Furthermore, there are considerable challenges in exploring the regulatory mechanism of the terrain–vegetation–atmosphere coupling system on regional climate variability. The local ecological response in mountainous areas is mismatched in temporal and spatial scales with large-scale climate forcing processes such as atmospheric circulation and monsoon activities, making it difficult to effectively separate natural climate variability from anthropogenic forcing signals and accurately disentangle the independent contributions of multiple driving factors.

Future research should prioritize the integration of long-term, full-coverage observational data across the entire Qinba Mountainous Region to reevaluate the impact mech-

anisms of climate cycles and terrain forcing on the atmospheric ecological pattern, with a focus on high-altitude ecologically sensitive zones [73]. Unraveling the teleconnection relationship between regional ecological evolution and global climate change remains a core scientific objective; supplementing multi-source auxiliary datasets such as aerosol concentration, pollutant emissions, and land use dynamics will help build a more comprehensive multi-dimensional driving attribution system [74].

As a linear time-series model, ARIMA has limited capacity to describe nonlinear extreme climate events [75]. In the future, it can be combined with machine learning models such as LSTM and random forests for multi-model ensemble prediction [75]. Subsequent research can adopt higher spatiotemporal resolution observational data and multi-index fusion modeling methods to optimize time-series data reconstruction techniques [76]. Combining long-term field observations with climate simulations can further quantify the individual contributions of natural climate variability, regional atmospheric circulation, and anthropogenic warming to the atmospheric ecological evolution in mountainous areas [77], clarifying the interaction mechanism between internal climate variability and anthropogenic environmental changes in mountainous systems.

5. Conclusions

Based on 60-year time-series multi-factor datasets covering the period 1965–2024, this study constructs an integrated research framework of multi-dimensional time-series diagnosis, mechanism-constrained prediction, dynamic hierarchical zoning and robustness testing. Taking Shangluo City in the eastern Qinling Mountains as the study area, a typical mid-latitude mountain located in the climatic transition zone, this research systematically clarifies the spatiotemporal evolution characteristics of its atmospheric ecosystem, the elevation-dependent warming mechanism, and the four-dimensional coupled negative feedback "topography–climate–vegetation–air quality" mechanism. This study produces replicable and comparable scientific incremental knowledge, breaking through the limitations of traditional static assessment at the mechanism level. The relevant conclusions both verify and extend the existing research on global mid-latitude mountains (including the Qinghai–Tibet Plateau, the Alps, the Rocky Mountains, etc.).

Regarding the multi-factor coupling mechanism, this study goes beyond traditional bivariate correlation analysis, systematically constructing and verifying the four-dimensional strongly coupled negative feedback mechanism of "topography–climate–vegetation–air quality". This confirms that topography acts as the fundamental regulating carrier, which constrains the spatial pattern of water and heat via vertical gradients and sheltering effects; climate drives vegetation development through the linkage of temperature, humidity and sunshine; high vegetation coverage improves air quality via dust retention, humidification and boundary layer regulation; and good air quality further maintains the structural and functional stability of the ecosystem, forming closed-loop mutual feedback and synergistic gain. This study quantitatively identifies the stable coupling relationships, with a significant negative correlation between elevation and air temperature ($r = -0.89$) and a significant negative correlation between vegetation coverage and air quality ($r = -0.76$), revealing the closed-loop mutual feedback pathway: "topography constrains water–heat pattern → climate drives vegetation growth → vegetation retains dust and increases humidity → air quality is improved → ecosystem stability is enhanced".

In terms of the spatiotemporal evolution mechanism, the study area exhibits a steady-state evolution pattern characterized by weak seasonal fluctuation, strong interannual variability, low spatiotemporal variability and high robustness. The regional air temperature shows significant elevation-dependent warming, while precipitation, humidity and sunshine remain generally stable without extreme abrupt changes. The atmospheric ecological index

presents a stable spatial pattern of being high in the southwest and low in the northeast, and the coefficient of variation in the atmospheric ecological index across the whole study area is lower than 0.03. Results from 1000 Monte Carlo simulations confirm that ecological zoning does not experience hierarchical leaps under climate disturbance scenarios. Driven by the combined effects of enclosed canyon topography, atmospheric radiative forcing, and the positive feedback of surface albedo, high-altitude counties (Zhashui and Zhen'an) exhibit higher warming rates than low-altitude basins. Continuous mountain masses and high vegetation coverage jointly form a topographic thermal buffering effect, which can effectively suppress abnormal temperature fluctuations and improve ecosystem stability. This finding revises the traditional understanding that high-altitude regions are more ecologically fragile from a mechanistic perspective. The above characteristics differ from the strong seasonal fluctuation and rapid degradation pattern of European cryosphere mountains, reflecting the unique stability mechanism shaped by the joint effect of "north–south transition zone + high vegetation coverage + topographic barrier", enriching our understanding of the types and patterns of ecological evolution of mid-latitude mountains worldwide.

In terms of methodology–mechanism integration, this study embeds physical prior constraints, including topography, vegetation and elevation, into the ARIMA time-series model, breaking through the "black box" limitation of traditional purely data-driven approaches and unifying statistical fitting and physical mechanism. It constructs an integrated framework of multi-dimensional diagnosis, prediction, zoning and robustness verification, which is equipped with four-layer quality control, including an ADF stationarity test, Ljung–Box white noise test, STL seasonal decomposition and residual normality test, to guarantee the mechanistic reliability of trend identification and prediction results. This paradigm is reproducible and transferable, providing a standardized assessment approach of "mechanism priority, data support and closed-loop verification" for similar mountains located in climatic transition zones.

Regarding regional understanding, this study revises the traditional perception that "high-altitude ecosystems are more fragile" from the mechanism level, confirming that under the combined effect of long-term ecological protection and topography–vegetation synergy, the eastern Qinling Mountains have formed an atmospheric ecosystem with high resilience, strong buffering capacity and low sensitivity; high-altitude areas are not ecological vulnerability hotspots, but core units of thermal buffering and ecological stability. This new cognition provides a mechanistic basis for shifting the focus of ecological protection in the Qinling Mountains from "passive restoration" to "active conservation of high-stability units". The research results can provide mechanistic support for ecological protection and restoration, as well as climate adaptation governance in the Qinling Mountains, and offer a generalizable paradigm for the atmospheric ecological assessment of similar ecologically sensitive mid-latitude mountains worldwide.

Author Contributions: Conceptualization, L.W. and J.C.; methodology, X.L.; software, J.C.; validation, H.L. and S.Z.; formal analysis, X.Z.; investigation, Y.G.; resources, S.Z.; data curation, H.L.; writing—original draft preparation, L.W. and J.C.; writing—review and editing, L.W.; visualization, X.L.; supervision, Y.G.; project administration, H.L.; funding acquisition, L.W. All authors have read and agreed to the published version of the manuscript.

Funding: This research was funded by the Education Department of Shaanxi Province and Shangluo University, grant numbers 24JT006 and 24SKY017, and the APC was funded by Shangluo University.

Data Availability Statement: All meteorological observation data used in this study are confidential internal data provided by Shangluo Meteorological Bureau, one of the authors of this study is affiliated with this institution, and data acquisition was conducted in compliance with regulations. In accordance with national meteorological data management regulations and confidentiality requirements, raw

national meteorological monitoring data are classified confidential and cannot be disclosed, uploaded or released publicly. All analytical results and statistical conclusions in this paper are authentic and valid, calculated strictly based on the confidential raw data. The complete research findings are fully presented and consistent with actual local conditions. Restricted by national data confidentiality rules, we cannot provide the original confidential data. Your understanding is appreciated.

Conflicts of Interest: The authors declare no conflicts of interest.

Appendix A

Table A1. Weight Determination Results of Atmospheric Ecological Evaluation Indicators in Shangluo City, Qinling Mountains Based on AHP-Expert Scoring Method.

Indicator Symbol	Indicator Name	Expert Average Score	Weight
T	Temperature	9.60	0.2483
AQI	Air Quality Index	9.45	0.2483
VC	Vegetation Coverage	7.95	0.1209
RH	Relative Humidity	8.80	0.1472
P	Precipitation	7.35	0.0930
SD	Sunshine Duration	6.95	0.0778
E	Altitude	6.70	0.0643

Notes: Weights were calculated by the Analytic Hierarchy Process (AHP) combined with expert scoring. Consistency ratio CR < 0.1 indicates valid weighting results.

$$AEI = 0.2483S_T + 0.2483S_{AQI} + 0.1209S_{VC} + 0.1472S_{RH} + 0.0093S_P + 0.0778S_{SD} + 0.0643S_E \quad (A1)$$

(ST, SAQI and other symbols represent scores of respective indicators; the scoring criteria are formulated based on the 60-year indicator distribution in Shangluo City).

The atmospheric ecological index (AEI) divides Shangluo City into four grades: Grade I (AEI > 8.0, excellent atmospheric ecological resources), Grade II (7.0 < AEI $\leq$ 8.0, good atmospheric ecological conditions), Grade III (6.0 < AEI $\leq$ 7.0, basically qualified atmospheric ecological conditions). The coefficient of variation (CV) is adopted to analyze grade stability. A CV value below 0.03 indicates high stability.

Table A2. 10-Level Evaluation Standards for Atmospheric Ecological Indicators in Shangluo City.

Score	Temperature (°C)	Relative Humidity (%)	AQI	Precipitation (mm)	Sunshine Duration (h)	Vegetation Coverage (%)	Altitude (m)
10	22.5–25.0	75–85	0–50	1490–1700	2200–2600	90–100	400–475
9	20.0–22.5	70–75	50–75	1350–1490	2000–2200	80–90	475–550
8	17.5–20.0	65–70	75–100	1280–1350	1800–2000	70–80	550–700
7	15.0–17.5	60–65	100–125	1150–1280	1600–1800	60–70	700–800
6	12.5–15.0	55–60	125–150	1070–1150	1400–1600	50–60	800–1000
5	10.0–12.5	50–55	150–175	970–1070	1200–1400	40–50	1000–1200
4	7.5–10.0	45–50	175–200	860–970	1000–1200	30–40	1200–1600
3	5.0–7.5	40–45	200–225	760–860	800–1000	20–30	1600–2000
2	2.5–5.0	35–40	225–250	650–760	600–800	10–20	2000–2200
1	0.0–2.5	30–35	250–300	540–650	400–600	0–10	2200–2400

Appendix B

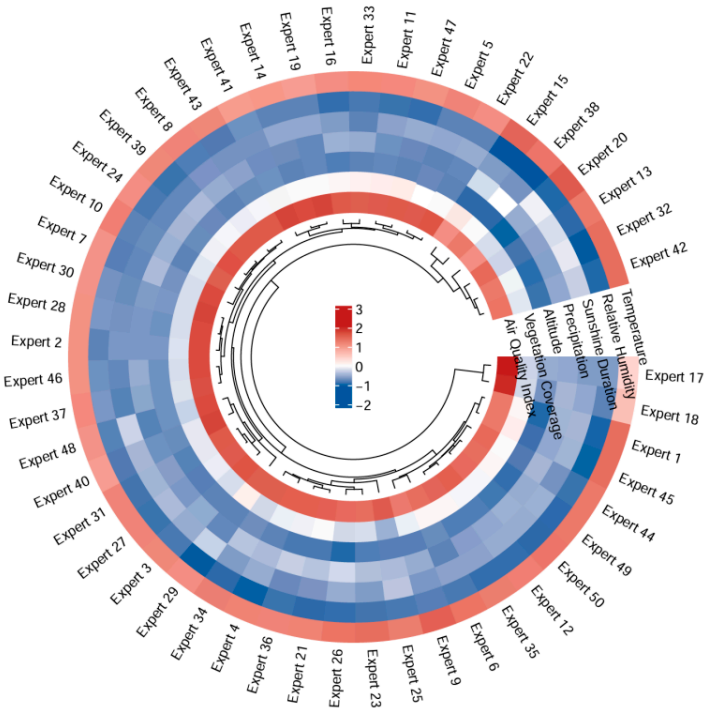

Figure A1. Correlation heatmap of scores assigned by 50 experts to 7 core atmospheric ecological indicators in Shangluo City. Note: All 50 selected experts have long been engaged in research and practical work related to mountain meteorology and climate, ecological environment and natural resource evaluation of the Qinling Mountains. The selection strictly follows four principles: professional matching, working years, research qualifications and regional adaptability. All experts hold associate senior professional titles or doctoral degrees with over 8 years of relevant research experience. They have long focused on climate evolution, atmospheric ecology and coupling mechanisms of vegetation and environment in Shangluo section of the Qinling Mountains, and are familiar with regional physical geography and meteorological observation characteristics. The experts come from universities, research institutes, meteorological departments and ecological environmental monitoring institutions, featuring rational professional composition and diverse research perspectives. They can ensure scientificity, objectivity and regional applicability of indicator scoring, and meet the professional evaluation requirements for weight assignment of the AHP analytic hierarchy process.

References

1. Katharina, A.; Werner, R.; Rupert, S. Climate change causes critical transitions and irreversible alterations of mountain forests. *Glob. Change Biol.* **2020**, *26*, 4013–4027. [CrossRef]
2. Zhao, C.; Yu, J.; Hou, Z.; Sun, H.; Zhang, Q.; Wang, Y.; Zhang, Z.; Gao, T.; Niu, T. Optimizing ecological security patterns in the Taihang Mountains based on ecosystem service synergies. *Environ. Sustain. Indic.* **2026**, *31*, 101292. [CrossRef]
3. Hu, Z.; Li, N.; Zhang, M.; Miao, M. Bayesian Network Analysis: Assessing and Restoring Ecological Vulnerability in the Shaanxi Section of the Qinling-Daba Mountains Under Global Warming Influences. *Sustainability* **2024**, *16*, 10021. [CrossRef]
4. Terzi, S.; Torresan, S.; Schneiderbauer, S.; Critto, A.; Zebisch, M.; Marcomini, A. Multi-risk assessment in mountain regions: A review of modelling approaches for climate change adaptation. *J. Environ. Manag.* **2019**, *232*, 759–771. [CrossRef]
5. Simon, J.; Marianne, E.; Erik, F.; Alexis, I.; Anders, L.; Hanne, S.; Anne, S.-T.; Paul, T.J.; Vigdis, V.; Guri, V.L.; et al. Introducing the index-based ecological condition assessment framework (IBECA). *Ecol. Indic.* **2021**, *124*, 107252. [CrossRef]
6. Canedoli, C.; Rota, N.; Vogiatzakis, I.N.; Zanchi, A.; Drius, M.; Nagendra, H.; Schioppa, E.P. Review of indicators for mountain ecosystem services: Are the most frequently used also the best? *Ecol. Indic.* **2024**, *166*, 112310. [CrossRef]
7. Rogora, M.; Frate, L.; Carranza, M.L.; Freppaz, M.; Stanisci, A.; Bertani, I.; Bottarin, R.; Brambilla, A.; Canullo, R.; Carbognani, M.; et al. Assessment of climate change effects on mountain ecosystems through a cross-site analysis in the Alps and Apennines. *Sci. Total Environ.* **2018**, *624*, 1429–1442. [CrossRef] [PubMed]

8. Liu, J.; Xie, T.; Lyu, D.; Cui, L.; Liu, Q. Analyzing the Spatiotemporal Dynamics and Driving Forces of Ecological Environment Quality in the Qinling Mountains, China. *Sustainability* **2024**, *16*, 3251. [CrossRef]
9. Xie, W.; Yao, Y. Quantifying human activity intensity in the Qinling-Daba Mountains. *People Nat.* **2024**, *6*, 1486–1501. [CrossRef]
10. Che, L.; Yin, S.; Jin, J.; Wu, W. Assessment and Simulation of Urban Ecological Environment Quality Based on Geographic Information System Ecological Index. *Land* **2024**, *13*, 687. [CrossRef]
11. Chao, S.; Li, J.; Liu, Y.; Cao, L.; Zheng, J.; Yang, Z.; Ye, J.; Li, Y. Ecological quality assessment and monitoring using a time-series remote sensing-based ecological index (ts-RSEI). *GISci. Remote Sens.* **2022**, *59*, 1793–1816. [CrossRef]
12. Zheng, Z.; Wu, Z.; Chen, Y.; Guo, C.; Francesco, M. Instability of remote sensing based ecological index (RSEI) and its improvement for time series analysis. *Sci. Total Environ.* **2022**, *814*, 152595. [CrossRef]
13. Yang, X.; Meng, F.; Fu, P.; Zhang, J.; Liu, Y. Instability of remote sensing ecological index and its optimisation for time frequency and scale. *Ecol. Inform.* **2022**, *72*, 101870. [CrossRef]
14. Xiao, X.; Guan, Q.; Zhang, Z.; Liu, H.; Du, Q.; Yuan, T. Investigating the underlying drivers of vegetation dynamics in cold-arid mountainous. *Catena* **2024**, *237*, 107831. [CrossRef]
15. Zhang, S.; Zhou, Y.; Yu, Y.; Li, F.; Zhang, R.; Li, W. Using the Geodetector Method to Characterize the Spatiotemporal Dynamics of Vegetation and Its Interaction with Environmental Factors in the Qinba Mountains, China. *Remote Sens.* **2022**, *14*, 5794. [CrossRef]
16. Qiao, B.; Cao, X.; Yang, H.; Wang, N.A.; Liu, X.; Zhou, B.; Zhao, H.; Liu, X.; Wang, Y.; Wang, Z.; et al. Nonlinear threshold effects of environmental drivers on vegetation cover in mountain ecosystems: From constraint mechanisms to adaptive management. *Ecol. Indic.* **2025**, *173*, 113328. [CrossRef]
17. Guo, J.; Kang, R.; Xu, T.; Deng, C.; Zhang, L.; Yang, S.; Si, L.; Kaufmann, H. A time-series-based remote sensing ecological index model for sustainable long-term ecological monitoring of desertification. *Int. J. Appl. Earth Obs. Geoinf.* **2025**, *143*, 104758. [CrossRef]
18. Xia, L.; Tan, H.; Zhang, J.; Yang, K.; Teng, C.; Huang, K.; Yang, J.; Cheng, T. Remote Sensing and Machine Learning Uncover Dominant Drivers of Carbon Sink Dynamics in Subtropical Mountain Ecosystems. *Remote Sens.* **2025**, *17*, 2843. [CrossRef]
19. Bai, J.; Wang, X.; Tu, Y.; Zhou, J.; Wang, X.; Yao, W.; Sun, Z. Integration of ecosystem service composite index and driving thresholds for ecological zoning management: A case study of Qinling-Daba Mountain, China. *J. Environ. Manag.* **2025**, *384*, 125309. [CrossRef]
20. Zhang, M.; Li, X.; Wang, L. An Adaptive Outlier Detection and Processing Approach Towards Time Series Sensor Data. *IEEE Access* **2019**, *7*, 175192–175212. [CrossRef]
21. Decorte, T.; Mortier, S.; Lembrechts, J.J.; Meysman, F.J.R.; Latré, S.; Mannens, E.; Verdonck, T. Missing Value Imputation of Wireless Sensor Data for Environmental Monitoring. *Sensors* **2024**, *24*, 2416. [CrossRef]
22. Li, N.; Wang, J. Comprehensive Eco-Environment Quality Index Model with Spatiotemporal Characteristics. *Sensors* **2022**, *22*, 9635. [CrossRef]
23. Jatinder, K.; Singh, P.K.; Sarbjit, S. Autoregressive models in environmental forecasting time series: A theoretical and application review. *Environ. Sci. Pollut. Res. Int.* **2023**, *30*, 19617–19641. [CrossRef]
24. Wang, X.; Wang, X.; Jin, X.; Kou, L.; Hou, Y. Evaluation and driving force analysis of ecological environment in low mountain and hilly regions based on optimized ecological index. *Sci. Rep.* **2024**, *14*, 24570. [CrossRef]
25. Bravo, R.Z.B.; Cunha, A.P.M.d.A.; Leiras, A.; Oliveira, F.L.C. A new approach for a drought composite index. *Nat. Hazards* **2021**, *108*, 755–773. [CrossRef]
26. Chen, X.; Chen, S.; He, Z.; Xue, D.; Fang, G.; Pan, K.; Fang, K. Developing a system for comprehensive regional Eco-environmental quality assessment in mountainous areas—A case study of Western Sichuan, China. *Front. Environ. Sci.* **2022**, *10*, 879662. [CrossRef]
27. Gómez-Limón, J.A.; Arriaza, M.; Guerrero-Baena, M.D. Building a Composite Indicator to Measure Environmental Sustainability Using Alternative Weighting Methods. *Sustainability* **2020**, *12*, 4398. [CrossRef]
28. Chen, Y.; Pun, C.S. An LM-Type Unit Root Test for Functional Time Series. *Mathematics* **2026**, *14*, 916. [CrossRef]
29. Alyousifi, Y.; Ibrahim, K.; Zin, W.Z.W.; Rathnayake, U. Trend analysis and change point detection of air pollution index in Malaysia. *Int. J. Environ. Sci. Technol.* **2022**, *19*, 7679–7700. [CrossRef]
30. He, H.; Gao, S.; Jin, T.; Sato, S.; Zhang, X. A seasonal-trend decomposition-based dendritic neuron model for financial time series prediction. *Appl. Soft Comput.* **2021**, *108*, 107488. [CrossRef]
31. Ying, Z.; Gong, M. Simulation of an Adaptive Model Based on AIC and BIC ARIMA Predictions. *J. Phys. Conf. Ser.* **2023**, *2449*, 012027. [CrossRef]
32. Zhao, L.; Li, Z.; Qu, L. Forecasting of Beijing PM2.5 with a hybrid ARIMA model based on integrated AIC and improved GS fixed-order methods and seasonal decomposition. *Heliyon* **2022**, *8*, e12239. [CrossRef]
33. Lu, Q.; Fan, H.; Zhang, F.; Chen, W.; Xia, Y.; Yan, B. The dominant role of human activity intensity in spatial pattern of ecosystem health in the Poyang Lake ecological economic zone. *Ecol. Indic.* **2024**, *166*, 112347. [CrossRef]
34. Sun, H.; Wang, J.; Xiong, J.; Bian, J.; Jin, H.; Cheng, W.; Li, A. Vegetation Change and Its Response to Climate Change in Yunnan Province, China. *Adv. Meteorol.* **2021**, *2021*, 8857589. [CrossRef]

35. Fernández-Martínez, M.; Vicca, S.; Janssens, I.A.; Carnicer, J.; Martín-Vide, J.; Peñuelas, J. The consecutive disparity index, *D*: A measure of temporal variability in ecological studies. *Ecosphere* **2018**, *9*, e02527. [CrossRef]
36. Yang, Y.; Song, G.; Lu, S. Assessment of land ecosystem health with Monte Carlo simulation: A case study in Qiqihaer, China. *J. Clean. Prod.* **2019**, *250*, 119522. [CrossRef]
37. Seifi, A.; Dehghani, M.; Singh, V.P. Uncertainty analysis of water quality index (WQI) for groundwater quality evaluation: Application of Monte-Carlo method for weight allocation. *Ecol. Indic.* **2020**, *117*, 106653. [CrossRef]
38. Vincenzo, M.; Caterina, G.; Stefano, M.; Monica, P. Does uncertainty in single indicators affect the reliability of composite indexes? An application to the measurement of environmental performances of Italian regions. *Ecol. Indic.* **2021**, *127*, 107740. [CrossRef]
39. Matteo, M.; Adriano, P. Normalization methods for spatio-temporal analysis of environmental performance: Revisiting the Min–Max method. *Environmetrics* **2022**, *33*, e2730. [CrossRef]
40. Zhang, L.; Liang, T.; Wei, X.; Wang, H. An improved indicator standardization method for multi-indicator composite evaluation: A case study in the evaluation of ecological civilization construction in China. *Environ. Impact Assess. Rev.* **2024**, *108*, 107600. [CrossRef]
41. Li, F.; Zhou, W.; Shao, Z.; Zhou, X.; Fu, X. Changes in landscape pattern and evaluation of ecosystem health in the Western Qinling Mountains from 2000 to 2018. *Acta Ecol. Sin.* **2023**, *43*, 1338–1352. [CrossRef]
42. Lan, X.; Li, W.; Tang, J.; Shakoor, A.; Zhao, F.; Fan, J. Spatiotemporal variation of climate of different flanks and elevations of the Qinling–Daba mountains in China during 1969–2018. *Sci. Rep.* **2022**, *12*, 6952. [CrossRef]
43. Li, Y.; Zhu, L.; Duan, Z.; Zhu, W.; Sulaiman, Y.A.; Ahtisham, A. Spatiotemporal distribution variation of extreme temperatures under elevation-dependent warming and its response characteristics to regional warming in Qinling-Daba Mountains, China. *J. Environ. Manag.* **2025**, *393*, 127067. [CrossRef]
44. Pepin, N.C.; Arnone, E.; Gobiet, A.; Haslinger, K.; Kotlarski, S.; Notarnicola, C.; Palazzi, E.; Seibert, P.; Serafin, S.; Schöner, W.; et al. Climate Changes and Their Elevational Patterns in the Mountains of the World. *Rev. Geophys.* **2022**, *60*, e2020RG000730. [CrossRef]
45. Lehner, M.; Rotach, M.W.; Sfyri, E.; Obleitner, F. Spatial and temporal variations in near-surface energy fluxes in an Alpine valley under synoptically undisturbed and clear-sky conditions. *Q. J. R. Meteorol. Soc.* **2021**, *147*, 2173–2196. [CrossRef]
46. Pepin, N.; Deng, H.; Zhang, H.; Zhang, F.; Kang, S.; Yao, T. An Examination of Temperature Trends at High Elevations Across the Tibetan Plateau: The Use of MODIS LST to Understand Patterns of Elevation-Dependent Warming. *J. Geophys. Res. Atmos.* **2019**, *124*, 5738–5756. [CrossRef]
47. Wei, S.; Wang, X.; Wang, K.; Liu, L.; Liang, B.; Zhao, W. Rethinking spatiotemporal variations in air temperature over the Qilian Mountains, Western China, from 1979 to 2018. *Atmos. Res.* **2023**, *286*, 106671. [CrossRef]
48. Beniston, M.; Farinotti, D.; Stoffel, M.; Andreassen, L.M.; Coppola, E.; Eckert, N.; Fantini, A.; Giacona, F.; Hauck, C.; Huss, M.; et al. The European mountain cryosphere: A review of its current state, trends, and future challenges. *Cryosphere* **2018**, *12*, 759–794. [CrossRef]
49. Zhao, P.; He, Z.; Du, J. Implications of elevation-dependent warming to water resources over the Chinese Qilian Mountains. *J. Water Clim. Change* **2023**, *14*, 239–252. [CrossRef]
50. Byrne, M.P.; Boos, W.R.; Hu, S. Elevation-dependent warming: Observations, models, and energetic mechanisms. *Weather Clim. Dyn.* **2024**, *5*, 763–777. [CrossRef]
51. Bretêcher, B.R.; Huang, Y.; Liu, L.; Gero, J. Strengthening Atmospheric Greenhouse Effect at the Arctic North Slope of Alaska Site Evidenced by Long-Term Records of the Downwelling Longwave Radiance Spectrum. *J. Geophys. Res. Atmos.* **2025**, *130*, e2025JD043680. [CrossRef]
52. Ding, C.; Shi, H.; Gao, Y.; Zheng, C.; Wu, Y.; Zhang, Y. The buffering effect of topographic microhabitats on regional temperature changes. *Acta Ecol. Sin.* **2023**, *43*, 5137–5149. [CrossRef]
53. Zhang, Y.; Bao, G.; Bao, Y.; Yuan, Z.; Rina, W.; Tong, S. Altitudinal Differences in Decreasing Heat Deficit at the End of the Growing Season of Alpine Grassland on the Qinghai–Tibetan Plateau from 1982 to 2022. *Land* **2025**, *14*, 758. [CrossRef]
54. Li, J.; Zhang, Y.; Yang, L.; Shan, Z. Seasonal variations in ecological environment quality across different geomorphological regions and their response mechanisms to climate change. *Sci. Rep.* **2025**, *15*, 26385. [CrossRef]
55. Dollinger, C.; Rammer, W.; Seidl, R. Climate change accelerates ecosystem restoration in the mountain forests of Central Europe. *J. Appl. Ecol.* **2023**, *60*, 2665–2675. [CrossRef]
56. Geng, S.; Shi, P.; Song, M.; Zong, N.; Zu, J.; Zhu, W. Diversity of vegetation composition enhances ecosystem stability along elevational gradients in the Taihang Mountains, China. *Ecol. Indic.* **2019**, *104*, 594–603. [CrossRef]
57. Chen, C.; Zhu, L.; Tian, L.; Li, X. Analysis of vegetation coverage change and driving factors of climate in the Qinba Mountain Area. *Acta Ecol. Sin.* **2019**, *39*, 3257–3266. [CrossRef]
58. Dong, Q.; Chen, C.; Yin, H.; Zhou, Y.; Zhu, L. Vegetation greenness characteristics and their responses to surface water and heat in the Qinba Mountains. *Acta Ecol. Sin.* **2023**, *43*, 1090–1101. [CrossRef]

59. Gnann, S.; Baldwin, J.W.; Cuthbert, M.O.; Gleeson, T.; Schwanghart, W.; Wagener, T. The Influence of Topography on the Global Terrestrial Water Cycle. *Rev. Geophys.* **2025**, *63*, e2023RG000810. [CrossRef]
60. Michael, M.; Alice, C.; Giacomo, B.; Maria, C.C.; Christoph, M.; Samuel, M.; Wolfgang, S.; Daniele, C.B.; Gabriele, C.; Ludovica, D.G.; et al. Observed snow depth trends in the European Alps: 1971 to 2019. *Cryosphere* **2021**, *15*, 1343–1382. [CrossRef]
61. Liu, W.; Wang, J.; Zuo, H.; Fu, Z.; Xiao, W.; Cui, Y.; Zhou, Z. Spatiotemporal Distribution and Variation Characteristics of Convective Activities in Different Climate Zones in Northern China Based on 25 Years of Satellite Observations. *Int. J. Climatol.* **2025**, *45*, e8908. [CrossRef]
62. Peng, J.; Peng, J.; Shen, Y.; Jin, Z.; Liu, T.; Li, Y.; Zhuang, J.; Wang, Z.; Yu, C.; Cheng, Y.; et al. Key Thoughts on the Research of the Ecological Geological Environment System of the Qinling Mountains. *Acta Ecol. Sin.* **2023**, *43*, 4344–4358. [CrossRef]
63. Yu, F.; Li, C.; Yuan, Z.; Luo, Y.; Yin, Q.; Wang, Q.; Hao, Z. How do mountain ecosystem services respond to changes in vegetation and climate? An evidence from the Qinling Mountains, China. *Ecol. Indic.* **2023**, *154*, 110922. [CrossRef]
64. He, H.; Ren, X.; Zhang, L.; Qin, K.; Feng, L.; Lyu, Y.; Niu, Z.; Zhang, M. Ecosystem assessment method based on "reference system—Current status—Change quantity". *Acta Ecol. Sin.* **2023**, *43*, 2049–2060. [CrossRef]
65. Yang, J.; Chen, Z.; Zhang, W.; Meng, G.; Cao, M.; Li, J.; Xu, C.; Wu, R.; Leng, H.; Wen, Q.; et al. Relationships among multiple ecosystem services in mountainous regions: A case study of the Gaoligong Mountains. *J. Environ. Manag.* **2025**, *387*, 125765. [CrossRef]
66. Zhai, H.; Yao, J.; Wang, G.; Tang, X. Study of the Effect of Vegetation on Reducing Atmospheric Pollution Particles. *Remote Sens.* **2022**, *14*, 1255. [CrossRef]
67. Guo, Q.; He, Z.; Wang, Z. Monthly climate prediction using deep convolutional neural network and long short-term memory. *Sci. Rep.* **2024**, *14*, 17748. [CrossRef] [PubMed]
68. Dong, Y.; Shi, X.; Sun, S.; Sun, J.; Hui, B.; He, D.; Chong, F.; Yang, Z. Co-evolution of the Cenozoic tectonics, geomorphology, environment and ecosystem in the Qinling Mountains and adjacent areas, Central China. *Geosyst. Geoenviron.* **2022**, *1*, 100032. [CrossRef]
69. Silva, R.P.; Zarpelão, B.B.; Cano, A.; Junior, S.B. Time Series Segmentation Based on Stationarity Analysis to Improve New Samples Prediction. *Sensors* **2021**, *21*, 7333. [CrossRef]
70. Tebaldi, C.; Debeire, K.; Eyring, V.; Fischer, E.; Fyfe, J.; Friedlingstein, P.; Knutti, R.; Lowe, J.; O'Neill, B.; Sanderson, B.; et al. Climate model projections from the Scenario Model Intercomparison Project (ScenarioMIP) of CMIP6. *Earth Syst. Dyn.* **2021**, *12*, 253–293. [CrossRef]
71. Tao, S. Model of Green Evaluation Index of Petrochemical Enterprises by Consistency AHP. *J. Phys. Conf. Ser.* **2019**, *1237*, 052008. [CrossRef]
72. Gong, Y.; Zhang, Y.; Wang, F.; Lee, C. Deep Learning for Weather Forecasting: A CNN-LSTM Hybrid Model for Predicting Historical Temperature Data. *Appl. Comput. Eng.* **2024**, *99*, 168–174. [CrossRef]
73. Duo, L.; Wang, J.; Zhang, F.; Xia, Y.; Xiao, S.; He, B.J. Assessing the Spatiotemporal Evolution and Drivers of Ecological Environment Quality Using an Enhanced Remote Sensing Ecological Index in Lanzhou City, China. *Remote Sens.* **2023**, *15*, 4704. [CrossRef]
74. Wang, J.; Chen, G.; Yuan, Y.; Fei, Y.; Xiong, J.; Yang, J.; Yang, Y.; Li, H. Spatiotemporal changes of ecological environment quality and climate drivers in Zoige Plateau. *Environ. Monit. Assess.* **2023**, *195*, 912. [CrossRef] [PubMed]
75. Qureshi, M.M.U.; Ahmed, A.B.; Dulmini, A.; Khan, M.M.H.; Rois, R. Developing a seasonal-adjusted machine-learning-based hybrid time-series model to forecast heatwave warning. *Sci. Rep.* **2025**, *15*, 8699. [CrossRef] [PubMed]
76. Xu, Z.; Sun, H.; Zhang, T.; Xu, H.; Wu, D.; Gao, J. The high spatial resolution Drought Response Index (HiDRI): An integrated framework for monitoring vegetation drought with remote sensing, deep learning, and spatiotemporal fusion. *Remote Sens. Environ.* **2024**, *312*, 114324. [CrossRef]
77. Wang, X.; Zhang, X.; Li, W.; Cheng, X.; Zhou, Z.; Liu, Y.; Wu, X.; Hao, J.; Ling, Q.; Deng, L.; et al. Quantitative Analysis of Climate Variability and Human Activities on Vegetation Variations in the Qilian Mountain National Nature Reserve from 1986 to 2021. *Forests* **2023**, *14*, 2042. [CrossRef]